PrP turnover in vivo and the time to effect of prion disease therapeutics

Taylor L Corridon[1], Jill O'Moore[2], Alyssa Seerley[2], Daniel A. Sprague[1], Yuan Lian[1], Vanessa Laversenne[1], Briana Noble[3], Nikita G Kamath[1], Fiona E Serack[1], Abdul Basit Shaikh[4], Brian Erickson[5], Craig Braun[5], Kendrick DeSouza-Lenz[6], Michael Howard[6], Nathan Chan[6], Walker S Jackson[7], Andrew G Reidenbach[1*], Deborah E Cabin[2], Sonia M Vallabh[1,8,9,10], Andrea Grindeland Panter[2], Nina Oberbeck[11], Hien T Zhao[3], Eric Vallabh Minikel[1,8,9,10†]

1. Program in Brain Health, Broad Institute of MIT and Harvard, Cambridge, MA, 02142, USA
2. Weissman Hood Institute, Great Falls, MT, 59405, USA
3. Ionis Pharmaceuticals, Carlsbad, CA, 92010, USA
4. Charles River Laboratories, Worcester, MA, 01605, USA
5. IQ Proteomics, Framingham, MA, 01702, USA
6. Comparative Medicine, Broad Institute of MIT and Harvard, Cambridge, MA, 02142, USA
7. Department of Biomedical and Clinical Sciences, Linköping University, Linköping, 581 83, Sweden
8. McCance Center for Brain Health and Department of Neurology, Massachusetts General Hospital, Boston, MA, 02114, USA
9. Department of Neurology, Harvard Medical School, Boston, MA, 02115, USA
10. Prion Alliance, Cambridge, MA, 02139, USA
11. Gate Bio, Brisbane, CA, 94005, USA

*Present address: Magnet Biomedicine, Boston, MA 02118, USA.
†Correspondence to eminikel@broadinstitute.org

Abstract

PrP lowering is effective against prion disease in animal models and is being tested clinically. Therapies in the current pipeline lower PrP production, leaving pre-existing PrP to be cleared according to its own half-life. We hypothesized that PrP's half-life may be a rate-limiting factor for the time to effect of PrP-lowering drugs, and one reason why late treatment of prion-infected mice is not as effective as early treatment. Using isotopically labeled diet with targeted mass spectrometry, as well as antisense oligonucleotide treatment followed by timed PrP measurement, we estimate a half-life of 5-6 days for PrP in the brain. PrP turnover is not affected by over- or under-expression. Mouse PrP and human PrP have similar turnover rates measured in wild-type or humanized knock-in mice. CSF PrP appears to mirror brain PrP in real time in rats. PrP is more readily quantifiable in colon than in other peripheral organs, and appears to have a shorter half-life in colon than in brain. An under-expressed pathogenic mutant PrP, corresponding to D178N in humans, exhibits an accelerated turnover rate. Our data may inform the design of both preclinical and clinical studies of PrP-lowering drugs.

Introduction

Pharmacologic lowering of prion protein (PrP) delays onset and slows progression of prion disease in animal models[1–3], consistent with PrP as the substrate for prion misfolding and the pivotal molecule in progression of this rapid neurodegenerative disease[4,5]. Inspired by this finding, a PrP-lowering antisense oligonucleotide (ASO) is now in a Phase I clinical trial (NCT06153966), with additional PrP-lowering modalities in preclinical development[6].

Prion disease typically presents as a rapidly progressive dementia[7]. With the median patient in prior clinical trials surviving just ~2 months from randomization[8,9], the time to effect of prion disease therapeutics could be a critical determinant of efficacy in the symptomatic population. In mouse models, PrP lowering is most effective when treatment is administered early in the silent

incubation period (<78 days post-inoculation or dpi)[1]. Treatment after frank symptoms emerge (132 – 143 dpi) has extended survival primarily by increasing the time that animals are sick, without reverting any symptoms already accumulated[1,2], and only a subset of late-treated animals benefit, while others succumb to disease on a similar timeframe as untreated animals[1]. One explanation is simply that PrP lowering cannot reverse existing neuronal loss. However, the observation that efficacy is limited even very late pre-symptomatic timepoints (105 – 120 dpi)[1] led us to speculate that PrP turnover may be another factor limiting the efficacy of late treatment. ASOs target the PrP RNA for cleavage and degradation by RNase H1[1,10,11], suppressing new PrP synthesis but leaving pre-existing PrP to be degraded according to its own half-life. PrP turns over rapidly in cultured cells[12,13], but in vivo, reports are conflicting. A study using oral doxycycline to suppress expression of PrP under a Tet-off transgene determined the half-life of normally folded cellular PrP (PrP^C) to be just 0.75 days in the brain[14], while 2 mass spectrometry studies of mice fed isotopically labeled chow determined half-life estimates of 4.95 or 5.02 days in the brain[15,16]. Given that prion disease has heterogeneous subtypes with distinct rates of progression[7], the difference between a half-life of <1 day versus 5 days would have a dramatic impact on the inclusion criteria needed to select for patients likely to have time to benefit from a PrP-lowering drug in clinical trials.

Here we set out to determine the half-life of PrP in brain, as well as to answer several related questions. Because some PrP-lowering drugs in development are expected to have systemic activity[6], we sought to identify an organ or tissue that could be used as a proxy for peripheral target engagement in preclinical models, and further to determine the PrP half-life and therefore timeline on which target engagement can be observed in such a tissue. To mitigate translational risk due to amino acid sequence differences, depth of target suppression, or disease state, we sought to determine whether PrP half-life differs between human versus mouse PrP, in heterozygous knockout versus overexpressing animals, or in prion-infected versus naïve animals. Because cerebrospinal fluid (CSF) is being used as a sampling compartment to reflect on brain PrP[5,17], we also sought to determine the timeframe on which brain target engagement can be read out in CSF. Finally, because pathogenic variants in neurodegenerative disease-associated proteins can impact protein half-life[18], we sought to determine whether the pathogenic D178N variant, which results in reduced PrP expression[19,20], alters PrP's half-life.

Results

We sought to identify a peripheral tissue in which we could quantify PrP. Analysis of human *PRNP* RNA expression data from Genotype-Tissue Expression project (GTEx v8)[21] revealed that after brain and sciatic nerve, colon was the next tissue with the highest *PRNP* expression (Figure 1A). We dissected 15 organs from 1 wild-type and 1 PrP knockout mouse and analyzed them by Western blot. Brain exhibited far more PrP than any peripheral organ examined, but a strong band was identified centered at the expected molecular weight (~37 kDa) in colon, with weaker bands in stomach, quadriceps, heart, femur, spleen, and uterus, and faintly detectable bands in lung, lymph node, and skin. PrP was not detectable in liver, kidney, whole blood, or plasma (Figure 1B). Although homogenization efficiency and total protein loading varied between organs, Coomassie analysis revealed that the WT and KO animals were similarly loaded for any given organ (Figure 1B). When the same tissues were analyzed at a 1:100 wt/vol final dilution by our in-house ELISA[17] with the EP1802Y/8H4 antibody pair, all tissues besides brain were near the lower limit of quantification (LLQ), with many reading above LLQ in the knockout animals, presumably due to matrix effects (Figure 1C). Of any organ where the knockout tissue read out at LLQ, colon exhibited the strongest PrP signal in the wild-type animal (Figure 1D). Colon and 4 tissues with weaker signal were re-analyzed at a 1:25 wt/vol final

dilution, yielding higher signal and confirming colon as the strongest tissue at 5-fold above LLQ (Figure 1E). Further assay development identified the best conditions for ELISA detection of colon PrP and established stability parameters for colon samples in this assay (Figure S1). These results led us to select colon as our proxy tissue.

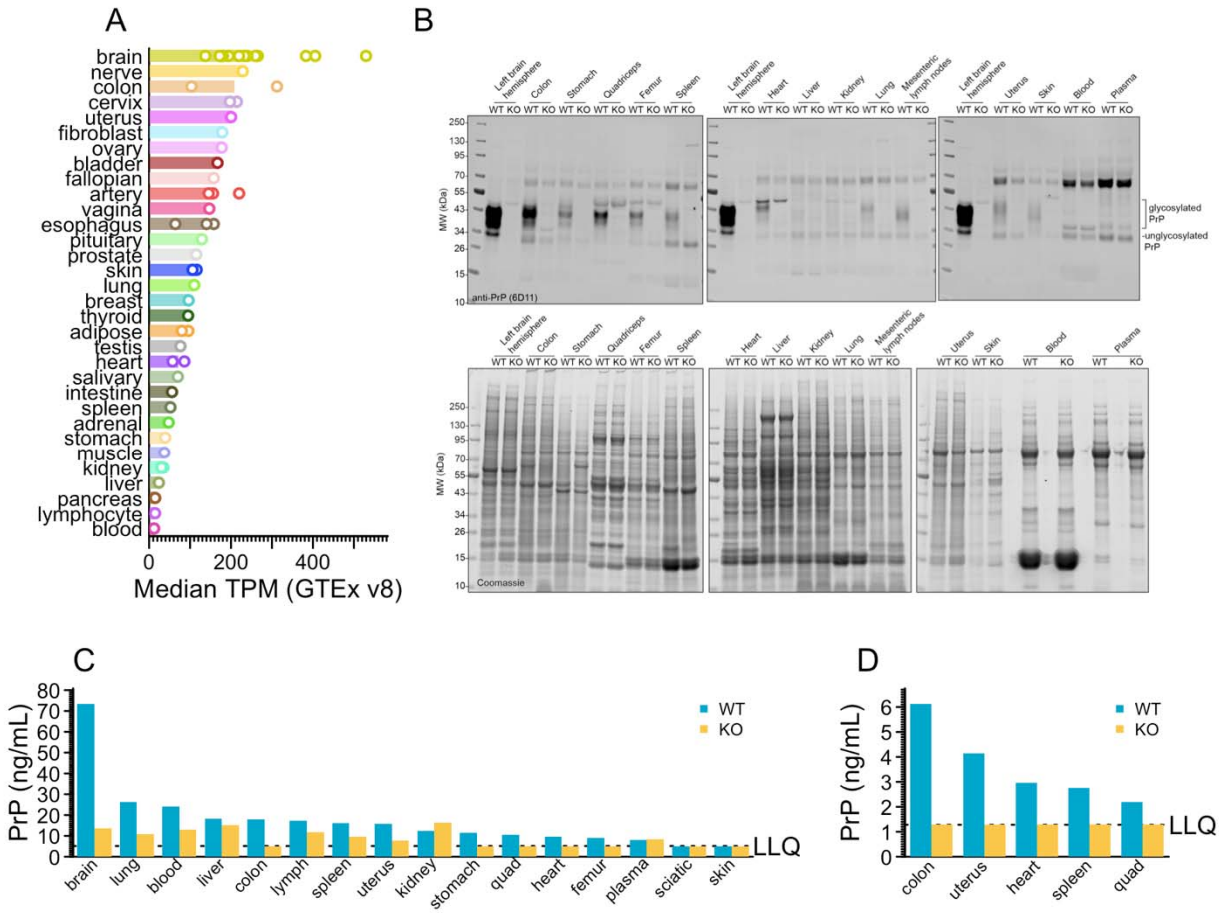

Figure 1. Nomination of colon as a tissue for peripheral PrP quantification. A) *PRNP RNA expression in transcripts per million (TPM) in human tissues according to GTEx v8 public data. Each sub-tissue (e.g. brain – cerebellum) is represented by one point as the median TPM across all samples for that tissue, and each tissue (e.g. brain) is represented by one bar as the median of those medians.* ***B)*** *Western blot (top) and Coomassie (bottom) of organs all from the same 1 WT and 1 KO animal, 6D11 anti-PrP antibody, see Methods for details.* ***C)*** *Organs tested by PrP ELISA at a 1:100 final dilution (10% homogenates at a further 1:10). PrP ELISA as reported except using double the detection mAb concentration (0.5 µg/mL instead of 0.25 µg/mL).* ***D)*** *Organs tested by PrP ELISA at a 1:25 final dilution (10% homogenates at a further 1:2.5). PrP ELISA as reported except using double the detection mAb concentration (0.5 µg/mL instead of 0.25 µg/mL). See Figure S1 for further assay development.*

We next sought to use targeted MS to measure turnover in both brain and colon. Initially we focused solely on the peptide VVEQMCVTQYQK (hereafter abbreviated VVEQ), the most readily quantified of any PrP tryptic peptide[22]. We fed wild-type mice with $^{13}C_6$ lysine chow, sacrificed them at 0, 2, 4, 6, or 8 days — a range of timepoints around the hypothesized half-life of PrP based on prior mass spectrometry studies[15,16] — measured VVEQ by targeted mass

spectrometry, and quantified the percent labeled as the ratio of heavy peptide to heavy plus light. Due to lower overall PrP abundance (Figure S1), the LLQ in colon occurred at 13.3% labeling versus 2.5% for brain; nonetheless, heavy peptide was above LLQ in most samples by day 2, and in all samples on days 4-8 (Figure 2A). Heavy labeled peptide accumulated much more quickly in colon than in brain, with the two tissues reaching 49.3% and 20.5% respectively by day 8 (Figure 2A), potentially suggesting a shorter half-life in colon than in brain.

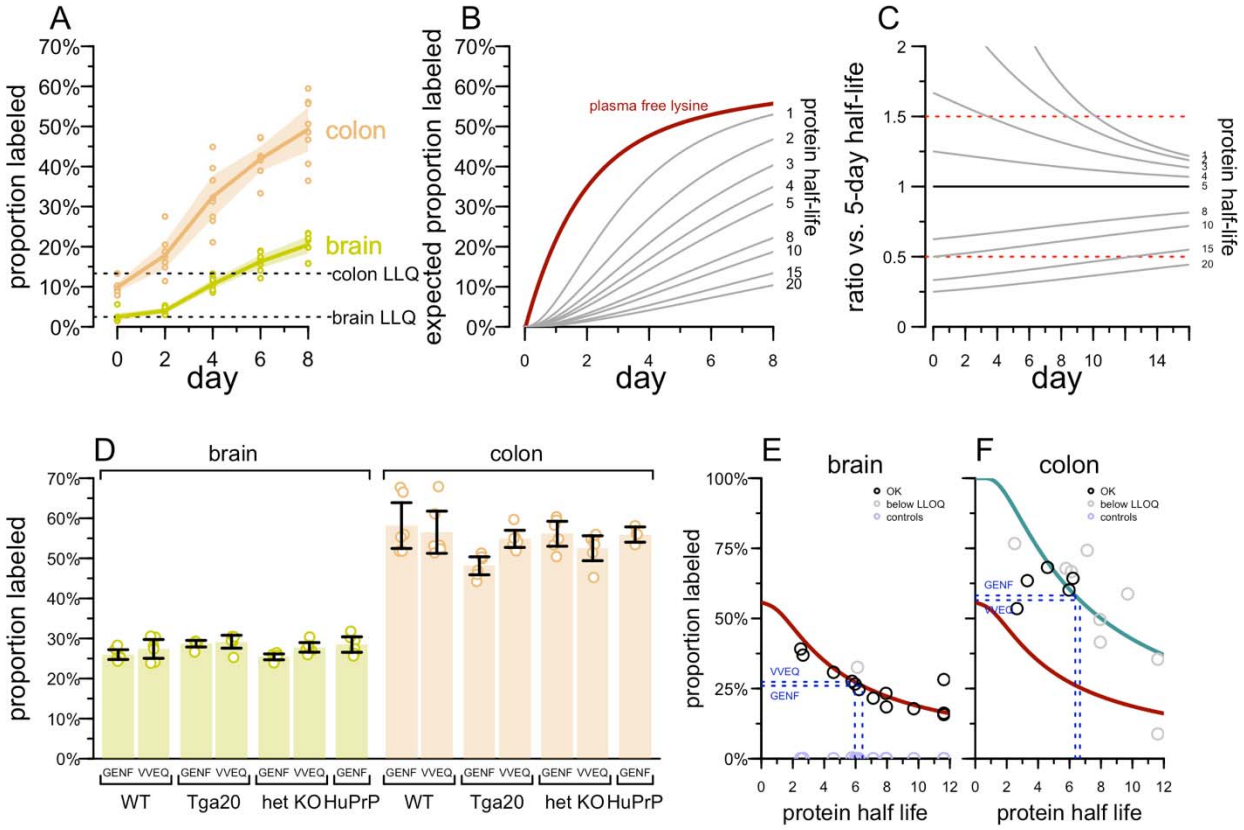

Figure 2. Determination of PrP half-life by targeted mass spectrometry. A) *Accumulation of $^{13}C_6$ label from chow in the VVEQ peptide in mouse brain and colon.* ***B)*** *The best fit to the proportion of plasma free lysine empirically found to be $^{13}C_6$ labeled, as reported by Fornasiero (maroon), and the proportion of peptide expected to be labeled over time as a function of half-life (shown in days on the right side). See Methods > Labeled peptide accumulation models for details.* ***C)*** *The ratio of proportion labeled (B) for a peptide of each half-life compared to a peptide of 5-day half-life. Ratios of 0.5 and 1.5 are arbitrary landmarks highlighted to orient the eyes to a straight horizontal line.* ***D)*** *The proportion of PrP peptides VVEQ and GENF that are $^{13}C_6$ labeled after 8 days as a function of mouse genotype. All differences are non-significant at Bonferroni-corrected P > 0.05, 2-sided T-test.* ***E)*** *Proportion labeled in brain (y axis) versus brain half-life previously reported by Fornasiero for all measured non-PrP peptides (circles); black = measured peptide signal above LLQ, gray = below LLQ. The maroon line represents the expected proportion labeled after 8 days as a function of half-life, based on the model from (B). The horizontal blue lines represent the proportion labeled observed for the two PrP peptides, and their vertical projection from the maroon curve down to the x axis represents the estimation of half-life from those proportion labeled measurements.* ***F)*** *As in (E), but for colon. The additional cyan curve represents the expected proportion labeled after 8 days if 100% of lysine available for protein synthesis is $^{13}C_6$ labeled at all times.*

In order to interpret these data, we considered implications of the mathematical model for heavy label accumulation presented by Fornasiero et al[16]. Fornasiero measured the proportion of free lysine in mouse plasma that was labeled, and fit a model represented by the maroon line (Figure 2B). In this model, the proportion of lysine that is heavy labeled rises rapidly initially as dietary lysine becomes bioavailable, but then increases more slowly, reaching 55.7% by day 8, because the labeled dietary lysine is in competition with unlabeled lysine made available by catabolism of endogenous proteins. Because only a portion of free lysine is labeled, calculating the expected proportion of a peptide labeled as a function of its protein's half-life revealed that according to this model, peptides from a protein with a 5-day half-life would be just 30.0% labeled by day 8, even though 62.1% of the protein would turn over in this time (Figure 2C).

With this in mind, we considered how many days of labeled chow consumption would best discriminate between shorter and longer half-lives. This analysis revealed a tradeoff: the theoretical difference between proportion labeled for a quick turnover protein and a slow turnover protein is maximized at early timepoints when the overall proportion labeled is still low enough that the precision of measurement near LLQ could be limiting. At later timepoints, the proportion labeled is higher, mitigating LLQ concerns, but the theoretical proportion labeled is less different. For discriminating half-lives near 5 days, an 8-day labeled chow experiment appeared to present a reasonable compromise between these tradeoffs.

To replicate and extend our results, we performed a multiplex targeted MS assay using VVEQ, another PrP peptide GENFTETDVK (hereafter abbreviated GENF), and a sampling of peptides from proteins whose brain half-lives as determined by Fornasiero[16] ranged from 2.5 to 11.6 days, to serve as controls. Serial dilution of $^{13}C_6$ $^{15}N_2$ lysine synthetic peptides for this assay identified lower limits of quantification (LLQ) for each peptide; the mean heavy peptide area found in wild-type mice after 8 days of labeled chow was above LLQ for 17 peptides in brain and for 8 in colon, indicating the suitability of these peptides for this purpose (Figure S2).

We utilized multiple mouse lines (Table 1) to determine the impact of PrP amino acid sequence and expression level on half-life. For the multiplex MS assay, we fed wild-type, heterozygous PrP knockout, transgenic humanized (Tg25109; human PrP 129M), and transgenic overexpressing (Tga20 mouse PrP) mice with $^{13}C_6$ lysine chow, sacrificed them at 8 days, and analyzed their brains by mass spectrometry. For either PrP peptide, measured in either tissue, the proportion labeled was not significantly different from wild-type for any genotype (Figure 2D).

Table 1. Mouse lines used in this study. **Maintained on a background of homozygous ZH3/ZH3 PrP knockout. **MoPrP-A refers to the mouse reference genome PrP sequence as found in C57BL/6N and most other commonly used mouse strains (as opposed to the MoPrP-B allele, containing the two substitutions L108F and V189T, found in certain strains[23]). ***The 3F4 epitope is two amino acid changes from the MoPrP-A sequence: L108M + V111M. ****Mean value obtained for 2 peptides in young and aged ki-3F4-FFI mice in Figure 4 of this study.*

Name	PrP amino acid sequence	Expression level (fold wild-type)	Genomic location	Reference
ZH3/+	MoPrP-A**	0.5x	*Prnp*	[24]
Tg25109*	HuPrP 129M	1.1x	*Frdm6/Tmx1*	[25]
Ki817	HuPrP 129V	1.0x	*Prnp*	This study Fig S5
Tga20*	MoPrP-A	2.4x	*Ptcra*	[26], this study Fig S6
ki-3F4-WT	MoPrP-3F4***	1.0x	*Prnp*	[27]

ki-3F4-FFI	MoPrP-3F4-D177N	0.4x****	*Prnp*	[27], this study Fig 4

When we plotted, for each peptide from various proteins, the proportion labeled in wild-type mouse brain at day 8 versus the half-life reported by Fornasiero (Figure 2E), we found excellent agreement with the theoretical proportion labeled expected based on the plasma free lysine curve (Figure 2C). Projecting the proportion labeled for the two PrP peptides (26.0% and 27.3% for GENF and VVEQ respectively) onto this curve (blue dashed lines) yielded estimates of 6.4 and 6.0 days respectively. Control mice fed unlabeled chow categorically had percent labeled at <0.5%, confirming specificity of the assay.

For colon, the proportion labeled at day 8 (58.2% and 56.5% for GENF and VVEQ respectively) was higher than even the proportion of plasma free lysine expected to be labeled at day 8 (55.7%), meaning that even if PrP turnover in colon were virtually instantaneous, the proportion labeled in colon could not be explained by the plasma free lysine model (Figure 2F). We considered the possibility that the colon absorbs lysine directly from the diet, bypassing the bloodstream. To test the extreme, we modeled the expected proportion labeled if 100% of lysine used for nascent protein synthesis is labeled from day 0 (cyan curve, Figure 2F). The proportion labeled for several peptides in colon aligned more closely with this curve than with the plasma lysine curve (maroon curve, Figure 2F), although data are limited because many of these brain-expressed proteins are below LLQ in colon. Under the extreme assumption that 100% of lysine were labeled from day 0, the PrP half-life inferred from this model would be 6.4 and 6.7 days for GENF and VVEQ respectively. These estimates are very close to the half-life estimates from brain, yet the assumption of 100% of lysine used for nascent protein synthesis being labeled instantly upon switching to heavy chow is implausible. If labeled lysine availability is higher in colon than in brain but still less than 100%, then our data would be consistent with somewhat more rapid turnover in colon than in brain, both for PrP and for a number of other brain-expressed proteins.

We also sought to determine PrP's half-life by an orthogonal method. We dosed naïve wild-type mice with 500 µg PrP-lowering active ASO 6[1] (Table 2) by intracerebroventricular (ICV) injection at day 0 and then performed serial sacrifice to measure *Prnp* RNA and PrP protein in whole hemispheres at various timepoints post-dose (Figure 3A). Maximal RNA suppression was achieved within 3 days, while protein lagged, reaching its nadir at 28 days (Figure 3A). When we fit an exponential decay curve to the data, we obtained a half-life estimate of 4.8 days. Interestingly, while the model assumes a single rate of decay, the data do not fit such a paradigm perfectly. On one hand, we observed more knockdown at early timepoints than is explainable by a simple exponential decay model. For example, PrP protein was already down to 84% residual at day 1, when the model still predicts 98% residual. Conversely, we observed less pharmacodynamic activity at later timepoints than the model would predict: 58% residual at day 14, when the model predicts 52%. This could suggest that bulk PrP in whole brain hemisphere does not represent a single population with a uniform decay rate (see Discussion).

Table 2. Antisense oligonucleotides used in this study. *Black: unmodified DNA (2'H). Orange: 2' methoxyethyl (2'MOE). Blue: 2'-4' constrained ethyl (cEt). Unmarked backbone linkages: phosphorothioate (PS). Linkages marked with o = phosphodiester (PO). mC: 5-methylcytosine.*

ASO	sequence and chemistry	target	ref
ASO 6	mCToTomCoTATTTAATGTmCAoGoTmCT	mouse/rat *Prnp* 3' UTR	[11]
ASO N	GTomCoAoToAoATTTTmCTTAGmCoTAmC	human/NHP *PRNP* intron	[28]

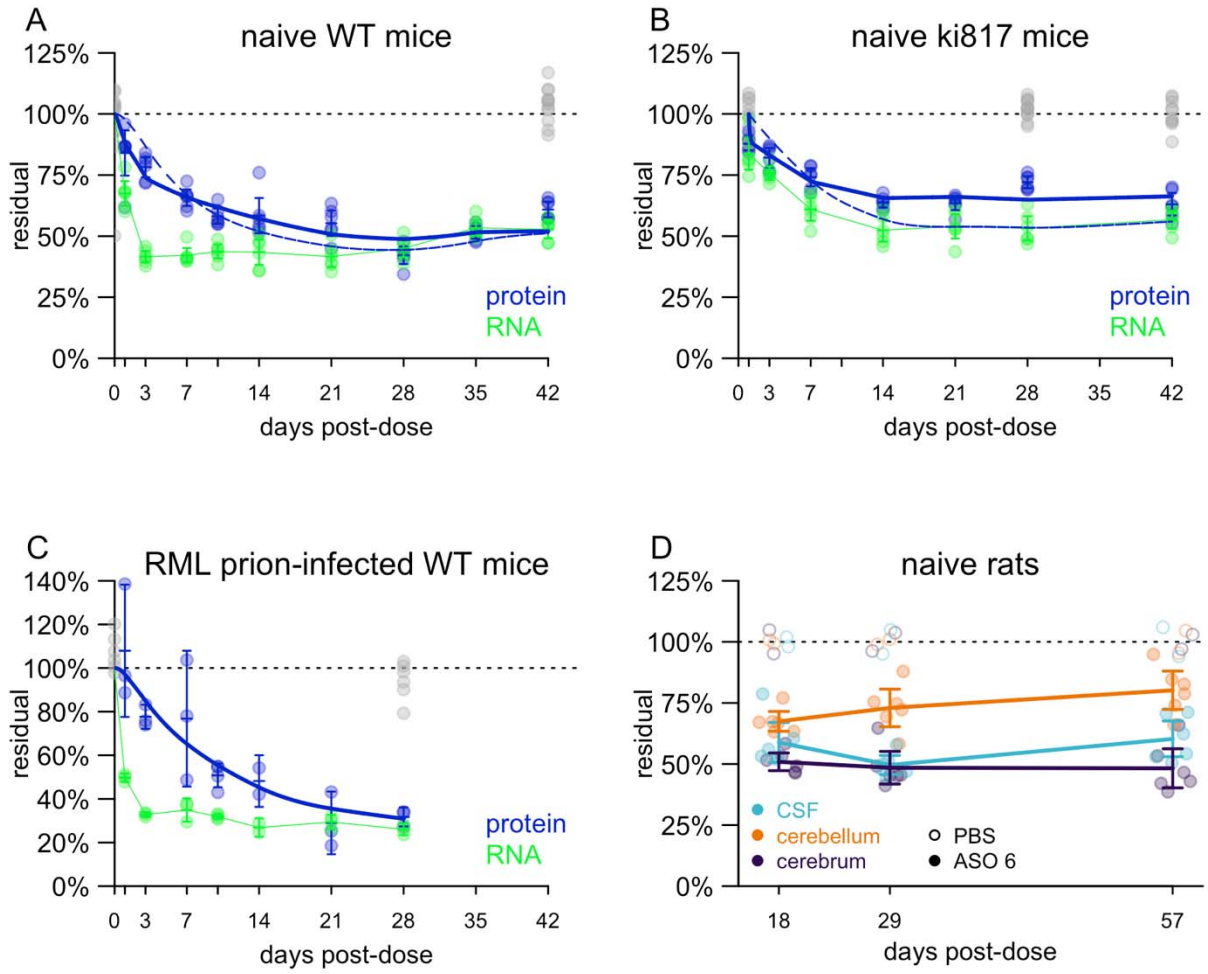

Figure 3. Determination of PrP half-life by ASO administration and timed sacrifice. A) *Residual Prnp RNA and PrP protein (y axis), normalized to the mean of saline controls, at various timepoints (x axis) for wild-type mice after a single ICV dose of 500 µg active ASO 6. Each point represents a whole brain hemisphere from one animal. All measurements in saline controls (both RNA and protein) are shown in gray. For each timepoint, line segments represent means and error bars represent 95% confidence intervals. The green curve represents linearly interpolated residual RNA concentration. The dashed blue curve represents a single-rate exponential decay model fit to the data. The solid blue curve represents a mixture-of-rates fit to the data.* ***B)*** *As in (A) but for Ki817 human PrP 129V knock-in mice after a single dose 118 µg of*

ASO N. ***C)*** *As in (A) but for wild-type mice infected with RML prions and treated with 300 µg ASO 6 at 105 dpi.* ***D)*** *Residual PrP in Sprague-Dawley rats treated with 1 mg of ASO 6 at day 0. Each point represents one animal, and for each timepoint, line segments represent means and error bars represent 95% confidence intervals. Long lines connect means of different timepoints.*

To confirm that there is no difference in half-life between mouse PrP and human PrP, we repeated the experiment in naïve humanized animals using a new human PrP (129V) knock-in mouse line termed Ki817 (Methods; Figure S4) treated with ASO N, which is potent against *PRNP* in both human and cynomolgus macaque[28]. Targeting 50% lowering to mirror the ASO 6 experiment above, we used a dose of 118 µg, which was the median effective dose (ED_{50}) estimated in mouse cortex[29]. Due to a shortage of these humanized mice, we included fewer late timepoints in this experiment, thus inadvertently biasing the model towards the early timepoints where, in our previous experiment, knockdown was deeper than predicted by exponential decay. Perhaps as a result of this bias, the estimated half-life from these data using the single-parameter model was just 2.1 days (solid blue curve, Figure 3B).

To determine whether prion infection affects the half-life of PrP, we also performed the same experiment in RML prion-infected wild-type mice with a single ICV dose of 300 µg active ASO 6 at 105 dpi (Figure 3C). This yielded a similar picture as in naïve mice, with a single-parameter half-life point estimate of 6.1 days. We note that we have not extensively tested the cross-reactivity of our PrP ELISA for PrP^{Sc}; given the non-denaturing conditions of our ELISA, our assay is likely measuring primarily or exclusively PrP^{C}.

To assess whether CSF PrP lags brain PrP, we used rats; the smaller CSF volume found in mice is challenging for robust PrP quantification[30]. After a single 1 mg ICV dose of active ASO 6 on day 0, rats were sacrificed at 18, 29, or 57 days post-dose and PrP was quantified in cerebrum (cortex and subcortex), cerebellum, and CSF (Figure 3D). Target engagement was deeper in cerebrum than in cerebellum at all timepoints, consistent with results from non-human primates and with the known difficulties in achieving strong ASO activity in cerebellar granule cells[28,31]. At all timepoints, the percent residual CSF PrP was in between that of cerebrum and of cerebellum, consistent with CSF reflecting some average of different brain regions. CSF PrP did not lag relative to cerebrum or cerebellum PrP, suggesting that it reflects brain PrP by 18 days post-dose, if not sooner.

Disease-causing missense variants in PrP have been shown to result in reduced PrP concentration in the CSF of asymptomatic humans at risk for prion disease[19,20] as well as in cultured cells and in the brain parenchyma of knock-in mice[27,32]. We sought to utilize a knock-in mouse model, ki-3F4-FFI, harboring the murine equivalent of the D178N variant, associated with low CSF PrP concentration in humans, to determine whether this underexpression results from accelerated turnover of PrP. Young (mean 9 weeks) or aged (mean 63 weeks) ki-3F4-FFI mice (Table 1; ref. [27]) were compared to age-matched wild-type C57BL/6N control animals as well as ki-3F4-WT, which additionally control for any impact of the 3F4 epitope as well as genetic background. All animals were fed isotopically labeled chow for 2, 4, 6, or 8 days and brains analyzed using the multiplex MS assay described above.

In young mice, the total amounts (regardless of isotopic label) of both PrP peptides (VVEQ and GENF) were reduced in the presence of the D178N substitution in ki-3F4-FFI mice, as expected (Figure 4A and S7), while decreases in abundance were not detected for any of the other proteins included in this multiplex assay. We fit empirical half-lives for every peptide in each mouse genotype; both PrP peptides exhibited significantly reduced half-lives (1.8 days for VVEQ and 2.4 days for GENF, versus 3.5 and 3.6 days respectively in control animals), while

significant changes were not detected for any other protein (Figure 4B). Examination of the accumulation of heavy lysine label in these two peptides (Figure 4C-D) revealed that the proportion of peptide labeled was already above either control mouse line after just 2 days of labeled chow. The relative difference between the ki-3F4-FFI and control mice did not further increase through day 8.

In aged mice, the total abundance of PrP peptides was again reduced in ki-3F4-FFI (Figure 4E and S7), confirming underexpression, however, no difference in half-life was detected (Figure 4F). The accumulation of heavy peptide over time in ki-3F4-FFI mice was indistinguishable for either peptide (Figure 4G-H).

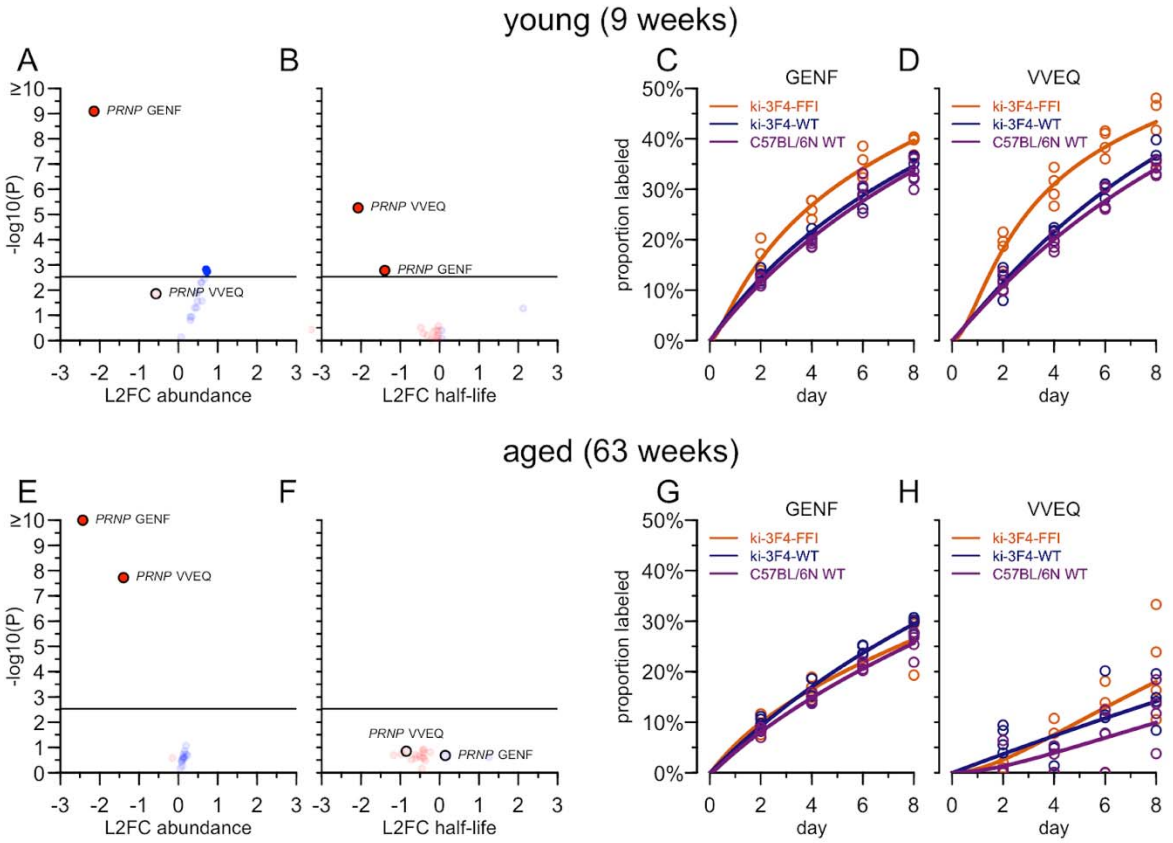

Figure 4. PrP turnover in mice with the equivalent of the D178N pathogenic variant by targeted mass spectrometry. A) *Peptide abundance across all young animals. Each point is one peptide included in this targeted MS assay. The x axis position is the log2 fold change in total intensity (light + heavy peptide) in ki-3F4-FFI animals (N=16) versus combined ki-3F4-WT and C57BL/6N animals (N=32 total). The y axis is -log10(P), with the P value from a 2-sided T-test.* ***B)*** *Half-life across all young animals. Each point is one peptide included in this targeted MS assay. A half-life is fit to the labeled chow days and proportion heavy peptide across all ki-3F4-FFI animals (N=4 per timepoint times 4 timepoints) and compared to that fit to the combined control groups (N=8 per timepoint times 4 timepoints). The x axis position is the log2 fold change in this estimated half-life. The y axis is -log10(P), with the P value of the main effect of genotype (ki-3F4-FFI vs. combined controls) in a beta regression model for proportion labeled*

peptide as a function of chow days. ***C)*** *Label accumulation in the GENF peptide by genotype. Each point is one animal. The x axis position is the number of days of labeled chow, the y axis position is the proportion of the GENF peptide that is heavy lysine labeled. Solid lines represent mixture-of-rates decay model fit to the data.* ***D)*** *As in C but for the VVEQ peptide.* ***E-H)*** *As in A-D but for aged, 63-week old mice.*

As observed in the PrP-lowering active ASO 6 experiment (Figure 3A), a single-rate model visibly failed to adequately fit the data, with a characteristic pattern of early underfitting followed by overfitting at later time points (Figure S8). Mixture-of-rates models were fit to the data and produced visibly tight fits to the data (Figure 4C,D,G,H). AIC favored the mixture-of-rates model in 9/12 cases, with the 3 exceptions all being VVEQ peptide in aged mice (Table S19). On average, the mixture-of-rates models suggest across the 9 remaining cases that a fast component comprises 27.3% [95% CI: 17.5% to 37.2%] of the total PrP population with a very short half-life of 0.068 days [95% CI: 0.01 days to 0.152 days]. The slow component was estimated to be on average 72.7% [95% CI: 62.8% to 82.5%] of the total PrP population with an average half-life of 6.80 days [95% CI: 5.26 days to 8.34 days].

Modeling indicated that the main effect of the ki-3F4-FFI genotype on proportion labeled peptide was highly significant (shown in Figure 4B) while the interaction term between genotype and days of labeled chow was non-significant, implying no additional effect of ki-3F4-FFI beyond the first 2 days.

Discussion

Our data indicate that PrP's half-life is between 4.8 to 6.4 days in brain parenchyma, regardless of PrP expression level, regardless of human or mouse PrP amino acid sequence, and regardless of prion infection status, when modeled as a homogenous population. Our estimate is in agreement with prior studies using mass spectrometry on the brains of mice fed isotopically labeled chow[15,16]. The conflicting report which determined a half-life of 0.75 days[14] was performed in a transgenic Tet-off mouse line with PrP under a foreign promoter[33]. That mouse line apparently exhibited a PrP expression pattern different from endogenous PrP, as evidenced by the perinatal lethality observed when PrP was not suppressed with doxycycline treatment during pregnancy[33]. This might account for the different result. The mouse model also overexpresses PrP, and the animals in that study were infected with prions, but our data argue that neither of these factors is likely to explain the lower half-life estimate. In prion-infected mice dosed at 105 dpi and harvested from 106 to 133 dpi, we measured a half-life similar to that in uninfected mice, suggesting that the reported[34] downregulation of normal PrP^C occurring by 120 dpi, if true, might not arise from accelerated turnover.

We find no evidence that CSF PrP lags brain PrP. In a previous study, where we analyzed only rat cerebrum (cortex and subcortex) we found that at 4 weeks post-dose, each 1% PrP lowering in CSF corresponded to 1.4% lowering in cerebrum[17]. Our present data, analyzing both cerebrum and cerebellum, indicate that this discrepancy might arise not from a lag in CSF PrP response to brain PrP concentration changes, but rather, from weaker target engagement in the cerebellum, which is also in contact with CSF.

We report that PrP in colon, while lower than brain, is quantifiable by ELISA. This is consistent with colon being the only tissue besides CNS and PNS to be affected in prion disease: patients with C-terminal truncating mutations that remove PrP's GPI anchor and cause a gain of function

through change in localization often experience chronic diarrhea misdiagnosed as inflammatory bowel disease for decades before the onset of peripheral neuropathy and then dementia[35,36]. Unlike those other peripheral tissues with lower PrP expression, colon is highly innervated; the relatively high PrP concentration there might reflect enteric nervous system expression. Colon PrP quantification could permit measurement of peripheral target engagement in animal studies of systemic PrP-lowering therapeutics. In mice fed isotopically labeled chow, heavy PrP peptide accumulates much faster in colon than in brain. This might indicate both more rapid turnover of PrP in colon, and higher availability of dietary labeled lysine in colon.

The D178N variant in PrP, which causes highly penetrant genetic prion disease in humans[37], results in diminished PrP concentration in CSF even in asymptomatic at-risk patients[19,20], and is also underexpressed in mouse brain and in cultured cells[27,32]. We therefore utilized the ki-3F4-FFI mouse model, which harbors the equivalent of this variant, to examine the effect of this amino acid substitution on PrP turnover. We confirmed underexpression of PrP in brain parenchyma, but observed accelerated PrP turnover only in young mice, where the half-life of mutant PrP was estimated at 1.8 – 2.4 days. In aged ki-3F4-FFI mice, PrP turnover was indistinguishable from control animals. This may provide partial support for the hypothesis that the mid- to late-life onset of genetic prion disease could be triggered by progressive malfunction in protein quality control that, in youth, helps to clear the mutant protein. Our data are not fully consistent with this hypothesis, however, because we still observed diminished steady state levels of mutant PrP even in aged animals. Regardless, our data suggest that mutant PrP will turn over faster, if anything, than wild-type PrP, and thus that the time to effect for a PrP-lowering drug will be shorter, if anything, in patients with genetic prion disease.

The diminution of PrP after ASO treatment is not perfectly modeled by a single exponential decay curve. Compared to the theoretical model, we observe deeper target engagement in the first few days after dosing than should be possible given that even the RNA has not been fully suppressed and less than one PrP protein half-life has passed; conversely, we observe less deep target engagement after 2-3 weeks than should be expected. Likewise, in mice with the equivalent of the D178N variant, which is underexpressed, all of the increase in heavy peptide accumulation after exposure to isotopically labeled chow accrued within the first 2 days. One interpretation is that there are multiple populations of PrP that degrade according to different kinetics: for example, PrP might have different half-lives on different cell types, in different subcellular compartments, or in different multimeric states. Our observations justify this interpretation because they match the predicted theoretical behavior of a ground truth heterogeneous population with fast and slow subpopulations modeled with a homogenous rate. In cases where the single rate models visibly fail to fit, model selection criteria such as AIC greatly preferred the mixture-of-rates model despite the penalty for increased model complexity. The half-life of the slow component in the heterogenous population is always going to be longer than a single rate estimate, and may thus point towards a need for later timepoints in some experiments.

Our study has limitations. We do not have a perfect explanation for the higher rate of isotopic label incorporation in colon compared to brain. While our data suggest that it arises both from higher availability of dietary leucine and from a shorter half-life of PrP and possibly other proteins in colon, we have not empirically measured free $^{13}C_6$ lysine in colon to confirm this. We also have not yet tested the kinetics of very deep PrP knockdown, below 50% residual. We lack a method for interrogating the half-life of PrP protein at the single cell level, so we do not know whether the rates may differ on distinct cell types. Findings in the ki-3F4-FFI mouse model we utilized here could be confounded by prion disease-related changes, particularly in the aged animals. In our colony we did not observe premature mortality in this mouse line and were

unable to identify any unambiguous histopathologic or biomarker signs of prion disease through >100 weeks of age[38], however, in other laboratories this mouse line has been reported to spontaneously produce transmissible prions and to develop a variety of behavioral abnormalities[27,39]. Perhaps the most important limitation of this study is our reliance on animal models: while we modeled human PrP in transgenic mice, we have not yet studied the half-life of PrP in humans.

Overall, our data confirm that PrP's half-life is one rate-limiting step in the time to effect of therapeutics that act by inhibiting PrP synthesis. Ideally, drugs targeting PrP production could one day be combined with drugs increasing PrP catabolism or blocking its conversion to a misfolded form; pharmacologic proof-of-concept for such approaches in vivo is lacking but more research is merited. In the meantime, some sponsors might choose to enrich for patients with relatively high functional scores or relatively slower-progressing genotypes in order to see the strongest effect in trials. Accelerating diagnosis through better neurologist awareness, rapid referral, and shortened turnaround times for diagnostic tests will be critical for reaching patients early enough to achieve sufficient target engagement while they still possess quality of life.

Methods

Animals. All animal experiments were approved by Institutional Animal Care and Use Committees (IACUC) at the Broad Institute (protocol 0162-05-17), Weissman Hood Institute (protocol 2024-AG-77) or Ionis Pharmaceuticals (protocol 2021-1176). All mice were of a pure C57BL/6N or mixed 6N/6J background. Details of ages and genotypes are provided in respective sections below. We utilized the ZH3 line of PrP knockout mice, the Tg25109 line of HuPrP 129M humanized mice, and the Tga20 line of PrP-overexpressing mice. Genotyping was performed by Transnetyx. Suggested primers for Tg25109 have been reported[25]. The Ki817 huPrP 129V mouse line is described here for the first time; see methods below and Figure S5. Tga20 mice were developed by Fischer et al[40]; the Tga20 transgene array was localized to the *Ptcra* gene locus by Taconic/Cergentis using targeted locus amplification (TLA)[41]; for details see Figure S6.

Generation of human PrP knock-in mice. Humanized KI *PRNP* mice (ki817) were generated by Taconic using ES cell targeting using CRISPR/Cas9. The targeting vector was constructed using human BAC RP11-61G12 for the human *PRNP* (129V) sequence and the mouse BAC RP23-369F12 for the homology arms. This targeting vector, a puromycin resistance cassette plasmid, and a plasmid containing Cas9 and guide RNAs against desired cut sites in the mouse genome were co-transfected into C57BL/6NTac embryonic stem cells. These were then selected, incorporated into embryos, and implanted to yield founders. The full targeting strategy is provided as a PDF in this study's online data repository. The gRNA sequences used to target the mouse genomic region to be replaced with the human sequence were GGTCTGCTGATCCGACAACG and TAGAAGCTATGATGAACACC. The exact coordinates of human sequence incorporated into the mouse span from 306 bp upstream of the transcription start site to 1 bp downstream of the transcription end site (Figure S5).

Isotopic labeling of mice. Where necessary, prior to study start, mice were consolidated into cages of a single genotype. Mice at Broad (wild-type, ZH3/+, Tga20 heterozygous, Tg25109 heterozygous on a ZH3/ZH3 background) were between ages of 21-23 weeks old. Mice at Weissman Hood Institute (ki-3F4-FFI, ki-3F4-WT, and C57BL/6N) were 59-60 days old (~9 weeks, young cohort) or 429-439 days old (~63 weeks, aged cohort) at the start of isotopic diet.

Mice first received fed Mouse Express (unlabeled) irradiated mouse feed (Cambridge Isotope Laboratories, USA) for 7 days at libitum (Broad) or 14 days (Weissman Hood Institute) to acclimate to the new diet. The next day, mice were switched to Mouse Express L-Lysine ($^{13}C_6$, 99%) irradiated mouse feed (Cambridge Isotope Laboratories, USA) ad libitum and were sacrificed after 8 days (Broad) or 2, 4, 6, or 8 days (Weissman Hood Institute). Animals had standard water access and no alternate food source was made available during the study. In the pilot study at Broad, one animal per genotype was set aside (not fed isotopic chow) as a representative control. In the pilot study, the amount of chow given each day was weighed prior to feeding and the remaining chow was weighed each day to estimate the amount of chow being eaten per animal per day. Animals were weighed on day 1 of unlabeled chow, day 1 of isotopically labeled chow and were harvested 24 hours after the last labeled chow refresh.

Organ harvest. Animals were weighed directly before harvesting. Animals were euthanized via CO_2 asphyxiation and disarticulation of the skull and cervical vertebrae was utilized as a secondary measure. Left and right brain hemispheres were collected by hemi-secting the full intact brain with a scalpel on ice, hemispheres were collected into separate tubes and flash frozen on dry ice. Left and right sciatic nerves were collected in length from the proximal hip to distal knee and flash frozen on dry ice. Colon sections were harvested in length from the caudal end of the ascending colon to the middle of the transverse colon and flash frozen on dry ice. All samples were stored at -80C and sent for LC-MS in the form of frozen, intact tissue.

Immunoblots. All samples were homogenized in cold PBS with 0.2% CHAPS. All organs were homogenized at 10% wt/vol, except for sciatic nerve, which was 5% wt/vol due to limited sample mass, and blood and plasma, which were not homogenized. Each sample was then diluted 4-fold into RIPA buffer (20 mM Tris-HCl pH 8.0, 140 mM NaCl, 1 mM EDTA, 1% Triton X-100, 0.1% SDS) with protease inhibitors (MilliporeSigma 4693159001), vortexed for 1 minute, centrifuged 14,000 x G for 10 minutes at 4°C and then supernatants were diluted a further 4-fold into 4X LDS (ThermoFisher NP0007) + 50 mM TCEP (ThermoFisher 77720) and incubated 5 minutes at 95°C. 10 µL of this solution was then loaded per lane and run on a SDS-PAGE gel (4-12% Bis-tris NuPAGE No. NP0323BOX) in MES buffer for 40 minutes at 180V. Proteins were either Coomassie stained or transferred to iBlot using 20V for 7 minutes, cooled for 3-5 minutes, blocked with TBS blocking buffer (Licor No. 927-60001) for 1 hour at room temperature. 6D11 anti-PrP primary antibody (Biolegend no. 808003) was diluted 1:1000 in TBS blocking buffer with 0.2% Tween and incubated overnight at 4°C. Blots were then rinsed 4x with TBST (5 minutes each with rocking), and goat anti-mouse IRDye 800CW (Licor No. 926-32210) was diluted 1:10,000 in TBS blocking buffer with 0.2% Tween, incubated 1 hour at room temperature with rocking, and washed 4x with TBST (5 minutes each with rocking). Blots were imaged at 800 and 700 nm on a Licor Odyssey CLx Infrared Imaging System.

Tissue homogenization for ELISA. Each brain hemisphere was added to a 7 mL Precellys tube with pre-loaded zirconium oxide beads (Precellys, Bertin, USA) and homogenized in ice cold 0.02% CHAPS in 1x PBS with protease inhibitors (1 Roche cOmplete tablet 4693159001, Millipore Sigma, USA, per 10 mL of buffer) using 3x 40 seconds pulses at 6,000 rpm in the Bertin Technologies Precellys Evolution Touch Homogenizer (Bertin, USA). The final protocol for colon homogenization (after optimization, see Figure S1) used 2 mL Precellys tubes and 5x 40 second pulses at 8,000 rpm. Homogenates were aliquoted into multiple 40 µL aliquots for protein analysis and 1 mL aliquots as a backup stock, flash frozen on dry ice and stored at -80°C until further analysis.

PrP ELISA. PrP concentration in the rat and murine brain hemispheres was measured using a previously published PrP ELISA[17]. The capture antibody, EP1802Y (ab52604, Abcam, USA), is

incubated in a clear 96-well plate overnight at 4C. After blocking and sample incubation, biotinylated 8H4 antibody (ab61409, Abcam, USA) is used for detection with streptavidin-HRP (Pierce High Sensitivity, 21130, Thermo Fisher Scientific, USA) and TMB substrate (7004P4, Cell Signaling Technology, USA). Brain homogenates and QCs were diluted to 1:200 final concentration for the assay; the final protocol for colon homogenization (after optimization in Figure S1) utilizes a 1:100 final dilution. Recombinant mouse PrP, (MoPrP23-231) prepared as described[42,43] was used for the standard curve. Average residual PrP was calculated by dividing the amount of residual PrP in each treated brain by the mean concentration of residual PrP in the vehicle and/or no dose control brains from the same study and time point. For the colon data in Figure 1D-E, the detection mAb concentration was doubled (0.50 µg/mL instead of 0.25 µg/mL), but with further assay development (Figure S1) we were able to revert to the original 0.25 µg/mL concentration and maintain the ~5-fold margin above LLQ.

Prnp qPCR. The qPCR procedure has been described previously[1]. *Prnp* RNA levels were normalized first to housekeeping gene *Ppia* then to the mean of PBS-treated controls. Primers are as follows. Prnp forward: TCAGTCATCATGGCGAACCTT, reverse: AGGCCGACATCAGTCCACAT, probe: CTACTGGCTGCTGGCCCTCTTTGTGACX. Ppia forward: TCGCCGCTTGCTGCA, reverse: ATCGGCCGTGATGTCGA, probe: CCATGGTCAACCCCACCGTGTTCX.

Mouse inoculation. Mouse inoculation has been described previously[1]. Animals were freehand inoculated halfway between the right ear and right eye, approximately 1 mm right of the midline, with 30 µL of a 1% (wt/vol) brain homogenate from terminally sick RML prion-infected mice.

Mouse intracerebroventricular (ICV) injection. Mouse ICV was similar to that described previously[1]. ASOs were diluted to 500 µg in a 10 µL dose volume in dPBS (Gibco 14190) and administered into CSF by bolus ICV injection in stereotaxis (ASI Instruments, SAS-4100). Positioning utilized 18° ear bars in ear canals and incisors in the mouse adapter tooth bar, adjusted to −8 mm. A 1 cm incision was made and the periosteum was scrubbed with sterile cotton-tipped applicators in order to reveal bregma. Drug was administered in Hamilton syringes (VWR 60376-172) fitted with 22-gauge Huber needles (VWR 82010-236). The needle was aligned to bregma and then moved 0.3 mm anterior, 1.0 mm right, and then downward either 3.0 mm past where the bevel disappeared into the skull or 3.1 mm past where the tip of the needle first touched the skull. Liquid was ejected over 10 seconds and the needle withdrawn 3 minutes later while applying downward pressure on the skull with a cotton-tipped applicator. Incisions were closed with a horizontal mattress stitch (Ethicon 661H suture). Animals recovered from the anesthesia in their home cages on a warming pad.

Rat ICV injection. The rat ICV injection was as described previously[17]. The procedure is similar to that for mice (see above) except that it utilizes 27° atraumatic ear bars (ASI Instruments, EB-927), with coordinates: riser –6 mm, 1 mm caudal, 1.5 mm right, 3.7 mm from the surface of the brain into the lateral ventricle. A bore hole was first drilled using a sterile 1 mm × 33 mm drill bit (McMaster Carr, 5058N51) in a hanging-style handpiece (McMaster Carr, 4454A14) held in a stereotactic handpiece holder (ASI Instruments, DH-1000). Injection volume was 30 µL in a

gastight 1710 small RN syringe (Hamilton 81030). Incision closure utilized 5-O monofilament suture (Ethilon 661G-RL).

Targeted mass spectrometry. Peptides terminating in lysine were nominated based on prior mass spectrometry work[22]. Single peptide quantification for VVEQMCVTQYQK (Figure 2A) was performed at Charles River Labs (Worcester, MA). Serial dilution experiments determined an LLQ of 0.111 ng/mL (ng of peptide per mL of homogenate), corresponding to 30.6 fmol/mg (fmol of peptide per mg of total protein). Multiplex quantification of VVEQMCVTQYQK, GENFTETDVK, and the control peptides from other proteins (Figure 2D-F) was performed at IQ Proteomics (Framingham, MA). Details of the LCMS methods are provided in the supplementary material.

Labeled peptide accumulation models. Free lysine in plasma was assumed to follow the fit described by Fornasiero[16]: H = 1-0.503*(exp(-t*ln(2)*0.799))-0.503*exp(-t*ln(2)/39.423), where H means the proportion of free lysine that is $^{13}C_6$ labeled, and exp(x) signifies e^x. Using this formula we calculated the percent labeled at every timepoint from 0 to 8 days using increments of dt = 0.01 days. We then calculated the accumulation of $^{13}C_6$ lysine label in peptides using numerical integration as follows. For parameter lambda (λ), defined as $\lambda = \ln(2)/t_{1/2}$ the turnover of protein in an arbitrarily small unit of time dt is λ*dt. For a 5-day half-life protein, for example, λ = ln(2)/5 = 0.14, so that every 0.01 days, 0.01*ln(2)/5 = 0.0014 (expressed as a proportion) or 0.14% of protein is catabolized, and 0.14% of the original amount is produced to replace it. The protein begins 100% unlabeled, and label accumulates as unlabeled protein is catabolized and a greater and greater proportion of the nascent protein is $^{13}C_6$ labeled. The `uniroot` function in R was used to perform the inverse operation — estimating a half-life from the observed proportion labeled, by minimizing the residuals between this numerical integration model and the actual data over 1 or more observed timepoints. To assess genotypic differences in label accumulation, we fit a beta regression model where proportion of peptide labeled is a function of days of isotopically labeled chow and genotypic group, with an interaction term: `betareg(prop_labeled ~ chow_days * grp)`. We chose a beta regression model because the proportion of peptide that is labeled is inherently constrained to be between 0 and 1 inclusive, which this model reflects. The main effect for the genotype group is interpreted to signify the difference in peptide labeling equally affecting all timepoints, while the interaction term is interpreted to signify the difference in label accumulation over the timepoints.

Exponential decay model. All residual *Prnp/PRNP* RNA and PrP protein measurements were normalized, respectively, to the mean RNA and protein measurements in the untreated animals across all timepoints so that all measurements are on a scale from 0% (complete knockdown) to 100% (normal levels). Observed *Prnp/PRNP* RNA measurements in brain were linearly interpolated using the `approx` function in R to yield point estimates of residual RNA at units of dt = 0.01 days. Similar to the approach described above, the residual protein (P) at any given timepoint was computed numerically as a function of RNA (R) and the exponential decay parameter $\lambda = \ln(2)/t_{½}$ value. Catabolism of protein is proportional to the amount of protein in the previous time increment, while synthesis of protein is proportional to RNA in the previous time increment. So, at any time t, the protein catabolized is $P_{t-1} * \lambda * dt$, and the protein synthesized is $R_{t-1} * \lambda * dt$. Thus, the change in protein $dP = R_{t-1} * \lambda * dt - P_{t-1} * \lambda * dt$. The amount of protein at time t is $P_t = P_{t-1} + dP$. With this function in hand, another function was written to calculate the residuals of the actual data as compared to this model. Then, the `nls.lm` function in R was used to determine the λ value that minimizes those residuals, this fitting the model. A time increment of dt=0.01 and a starting guess of λ = 0.14, corresponding to a half-life of 5 days, were used in fitting the model.

Mixture-of-rates models. To test whether protein pools exhibit heterogeneous turnover kinetics, we fit two-component mixture models to both isotopic labeling and residual decay data. For isotopic labeling, the mixture model assumes the peptide pool comprises two subpopulations with distinct half-lives ($t_{½,1}$ and $t_{½,2}$) and proportions (π_1 and π_2 where $\pi_1 + \pi_2 = 1$). Label accumulation in each subpopulation was computed independently using the numerical integration approach described above, and the total proportion labeled was calculated as the weighted average $\pi_1 \cdot L_1(t) + \pi_2 \cdot L_2(t)$, where $L_1(t)$ and $L_2(t)$ represent label accumulation in the fast and slow pools, respectively. For residual decay experiments, the mixture model similarly assumes two protein pools with distinct decay rate constants (λ_1 and λ_2) and initial proportions (w_1 and w_2). Each pool's dynamics follow $dPk/dt = \lambda k \cdot R(t) \cdot wk - \lambda k \cdot Pk(t)$, with total protein $P(t) = P_1(t) + P_2(t)$. Mixture models were fit using the Nelder-Mead optimization algorithm with multiple starting parameter combinations to ensure robust as possible optimization. Model selection between single-rate and mixture models was performed using the Akaike Information Criterion ($AIC = n \cdot \ln(RSS/n) + 2k$) and Bayesian Information Criterion ($BIC = n \cdot \ln(RSS/n) + k \cdot \ln(n)$), where n is the number of observations, RSS is the residual sum of squares, and k is the number of model parameters. For the single-rate model, k = 2 (λ and σ) for residual decay or k = 1 ($t_{½}$) for isotopic labeling; for the mixture model, k = 4 (λ_1, λ_2, w_1, and σ) for residual decay or k = 3 ($t_{½,1}$, $t_{½,2}$, and π_1) for isotopic labeling. $\Delta AIC < -3$ was interpreted as substantial evidence favoring the mixture model. For mixture models, the effective half-life was calculated as the time at which the combined pool reaches 50% of its initial state by numerically solving $\Sigma(w_i \cdot 0.5^{(t/t_{½,i})}) = 0.5$.

Statistics, source code and data availability. All analyses were conducted using custom scripts in R 4.4.1, and the mixture-of-rates decay models fit using Julia 1.12.4. Exponential decay and label accumulation models are described above. Differences between genotypes in Figure 2 were compared using a 2-sided T test and Bonferroni corrected for 10 tests. Differences in peptide abundance between genotypes in Figure 4 were compared using a 2-sided T-test, while differences in labeled peptide accumulation were assessed using a beta regression model (see above). All error bars or shaded areas shown are 95% confidence intervals. P values of < 0.05 were considered significant. Raw data and source code sufficient to reproduce all figures and statistics in this manuscript will be made available at github.com/vallabhminikel/halflife.

Acknowledgments

This study was funded by the National Institutes of Health (R01 NS132022 to EVM and COBRE P20 GM152335 to AG), Prion Alliance, Ionis Pharmaceuticals, and Gate Bio.

Competing interests

BE and CB are employees of IQ Proteomics. ABS is an employee of Charles River Laboratories. NO is an employee and shareholder of Gate Bio. HTZ and BN are employees and shareholders of Ionis Pharmaceuticals. EVM has received speaking fees from Abbvie, Eli Lilly, Novartis, Vertex, and Voyager; consulting fees from Alnylam, Deerfield, and Regeneron; and research support from Cenos, Eli Lilly, Gate Bio, Ionis, and Sangamo Therapeutics. SMV acknowledges speaking fees from Abbvie, Biogen, Eli Lilly, Illumina, Ultragenyx, and Voyager; consulting fees from Alnylam, Invitae, and Regeneron; research support from Cenos, Eli Lilly, Gate Bio, Ionis, and Sangamo Therapeutics.

Author contributions

Designed the experiments: TLC, ABS, BE, CB, AGR, WSJ, AGP, SMV, NO, HTZ, EVM. Performed the experiments: TLC, JOM, AS, VL, BN, NGK, FES, ABS, BE, CB, KL, MH, NC, AGR, DEC. Supervised the research: SMV, AGP, NO, HTZ, EVM. Analyzed the data: TLC, DAS, YL, ABS, CB, NO, HTZ, EVM. Drafted the manuscript: TLC, DAS, ABS, CB, EVM. Reviewed and approved the final manuscript: all authors.

References

1. Minikel EV, Zhao HT, Le J, O'Moore J, Pitstick R, Graffam S, Carlson GA, Kavanaugh MP, Kriz J, Kim JB, Ma J, Wille H, Aiken J, McKenzie D, Doh-Ura K, Beck M, O'Keefe R, Stathopoulos J, Caron T, Schreiber SL, Carroll JB, Kordasiewicz HB, Cabin DE, Vallabh SM. Prion protein lowering is a disease-modifying therapy across prion disease stages, strains and endpoints. Nucleic Acids Res. 2020 Aug 10; PMID: 32776089

2. Raymond GJ, Zhao HT, Race B, Raymond LD, Williams K, Swayze EE, Graffam S, Le J, Caron T, Stathopoulos J, O'Keefe R, Lubke LL, Reidenbach AG, Kraus A, Schreiber SL, Mazur C, Cabin DE, Carroll JB, Minikel EV, Kordasiewicz H, Caughey B, Vallabh SM. Antisense oligonucleotides extend survival of prion-infected mice. JCI Insight. 2019 30;5. PMID: 31361599

3. Nazor Friberg K, Hung G, Wancewicz E, Giles K, Black C, Freier S, Bennett F, Dearmond SJ, Freyman Y, Lessard P, Ghaemmaghami S, Prusiner SB. Intracerebral Infusion of Antisense Oligonucleotides Into Prion-infected Mice. Mol Ther Nucleic Acids. 2012;1:e9. PMCID: PMC3381600

4. Prusiner SB. Prions. Proc Natl Acad Sci U S A. 1998 Nov 10;95(23):13363–13383. PMCID: PMC33918

5. Vallabh SM, Minikel EV, Schreiber SL, Lander ES. Towards a treatment for genetic prion disease: trials and biomarkers. Lancet Neurol. 2020 Apr;19(4):361–368. PMID: 32199098

6. Wadman M. Foiling deadly prions. Science [Internet]. Science; 2024 Mar 22 [cited 2024 Oct 9];383(6689). Available from: https://pubmed.ncbi.nlm.nih.gov/38513035/ PMID: 38513035

7. Pocchiari M, Puopolo M, Croes EA, Budka H, Gelpi E, Collins S, Lewis V, Sutcliffe T, Guilivi A, Delasnerie-Laupretre N, Brandel JP, Alperovitch A, Zerr I, Poser S, Kretzschmar HA, Ladogana A, Rietvald I, Mitrova E, Martinez-Martin P, de Pedro-Cuesta J, Glatzel M, Aguzzi A, Cooper S, Mackenzie J, van Duijn CM, Will RG. Predictors of survival in sporadic Creutzfeldt-Jakob disease and other human transmissible spongiform encephalopathies. Brain J Neurol. 2004 Oct;127(Pt 10):2348–2359. PMID: 15361416

8. Geschwind MD, Kuo AL, Wong KS, Haman A, Devereux G, Raudabaugh BJ, Johnson DY, Torres-Chae CC, Finley R, Garcia P, Thai JN, Cheng HQ, Neuhaus JM, Forner SA, Duncan JL, Possin KL, Dearmond SJ, Prusiner SB, Miller BL. Quinacrine treatment trial for sporadic Creutzfeldt-Jakob disease. Neurology. 2013 Dec 3;81(23):2015–2023. PMCID: PMC4211922

9. Haïk S, Marcon G, Mallet A, Tettamanti M, Welaratne A, Giaccone G, Azimi S, Pietrini V, Fabreguettes JR, Imperiale D, Cesaro P, Buffa C, Aucan C, Lucca U, Peckeu L, Suardi S, Tranchant C, Zerr I, Houillier C, Redaelli V, Vespignani H, Campanella A, Sellal F, Krasnianski A, Seilhean D, Heinemann U, Sedel F, Canovi M, Gobbi M, Di Fede G, Laplanche JL, Pocchiari M, Salmona M, Forloni G, Brandel JP, Tagliavini F. Doxycycline in Creutzfeldt-Jakob disease: a phase 2, randomised, double-blind, placebo-controlled trial. Lancet Neurol. 2014 Feb;13(2):150–158. PMID: 24411709

10. Wu H, Lima WF, Zhang H, Fan A, Sun H, Crooke ST. Determination of the role of the human RNase H1 in the pharmacology of DNA-like antisense drugs. J Biol Chem. 2004 Apr 23;279(17):17181–17189. PMID: 14960586

11. Reidenbach AG, Minikel EV, Zhao HT, Guzman SG, Leed AJ, Mesleh MF, Kordasiewicz HB, Schreiber SL, Vallabh SM. Characterization of the Prion Protein Binding Properties of Antisense Oligonucleotides. Biomolecules. 2019 Dec 18;10(1). PMID: 31861275

12. Caughey B, Race RE, Ernst D, Buchmeier MJ, Chesebro B. Prion protein biosynthesis in scrapie-infected and uninfected neuroblastoma cells. J Virol. 1989 Jan;63(1):175–181. PMCID: PMC247670

13. Borchelt DR, Scott M, Taraboulos A, Stahl N, Prusiner SB. Scrapie and cellular prion proteins differ in their kinetics of synthesis and topology in cultured cells. J Cell Biol. 1990 Mar;110(3):743–752. PMCID: PMC2116048

14. Safar JG, DeArmond SJ, Kociuba K, Deering C, Didorenko S, Bouzamondo-Bernstein E, Prusiner SB, Tremblay P. Prion clearance in bigenic mice. J Gen Virol. 2005 Oct;86(Pt 10):2913–2923. PMID: 16186247

15. Price JC, Guan S, Burlingame A, Prusiner SB, Ghaemmaghami S. Analysis of proteome dynamics in the mouse brain. Proc Natl Acad Sci U S A. 2010 Aug 10;107(32):14508–14513. PMCID: PMC2922600

16. Fornasiero EF, Mandad S, Wildhagen H, Alevra M, Rammner B, Keihani S, Opazo F, Urban I, Ischebeck T, Sakib MS, Fard MK, Kirli K, Centeno TP, Vidal RO, Rahman RU, Benito E, Fischer A, Dennerlein S, Rehling P, Feussner I, Bonn S, Simons M, Urlaub H, Rizzoli SO. Precisely measured protein lifetimes in the mouse brain reveal differences across tissues and subcellular fractions. Nat Commun. 2018 Oct 12;9(1):4230. PMCID: PMC6185916

17. Mortberg MA, Zhao HT, Reidenbach AG, Gentile JE, Kuhn E, O'Moore J, Dooley PM, Connors TR, Mazur C, Allen SW, Trombetta BA, McManus A, Moore MR, Liu J, Cabin DE, Kordasiewicz HB, Mathews J, Arnold SE, Vallabh SM, Minikel EV. Regional variability and genotypic and pharmacodynamic effects on PrP concentration in the CNS. JCI Insight. 2022 Mar 22;7(6):e156532. PMCID: PMC8986079

18. Crisp MJ, Mawuenyega KG, Patterson BW, Reddy NC, Chott R, Self WK, Weihl CC, Jockel-Balsarotti J, Varadhachary AS, Bucelli RC, Yarasheski KE, Bateman RJ, Miller TM. In vivo kinetic approach reveals slow SOD1 turnover in the CNS. J Clin Invest. 2015 July 1;125(7):2772–2780. PMCID: PMC4563686

19. Vallabh SM, Minikel EV, Williams VJ, Carlyle BC, McManus AJ, Wennick CD, Bolling A, Trombetta BA, Urick D, Nobuhara CK, Gerber J, Duddy H, Lachmann I, Stehmann C, Collins SJ, Blennow K, Zetterberg H, Arnold SE. Cerebrospinal fluid and plasma biomarkers in individuals at risk for genetic prion disease. BMC Med. 2020 June 18;18(1):140. PMCID: PMC7302371

20. Vallabh SM, Mortberg MA, Allen SW, Kupferschmid AC, Kivisakk P, Hammerschlag BL, Bolling A, Trombetta BA, Devitte-McKee K, Ford AM, Sather LE, Duffy G, Rivera A, Gerber J, McManus AJ, Minikel EV, Arnold SE. Fluid Biomarkers in Individuals at Risk for Genetic

Prion Disease up to Disease Conversion. Neurology. 2024 July 23;103(2):e209506. PMCID: PMC11226308

21. GTEx Consortium. The GTEx Consortium atlas of genetic regulatory effects across human tissues. Science. 2020 Sept 11;369(6509):1318–1330. PMCID: PMC7737656

22. Minikel EV, Kuhn E, Cocco AR, Vallabh SM, Hartigan CR, Reidenbach AG, Safar JG, Raymond GJ, McCarthy MD, O'Keefe R, Llorens F, Zerr I, Capellari S, Parchi P, Schreiber SL, Carr SA. Domain-specific quantification of prion protein in cerebrospinal fluid by targeted mass spectrometry. Mol Cell Proteomics MCP. 2019 Sept 26; PMID: 31558565

23. Westaway D, Goodman PA, Mirenda CA, McKinley MP, Carlson GA, Prusiner SB. Distinct prion proteins in short and long scrapie incubation period mice. Cell. 1987 Nov 20;51(4):651–662. PMID: 2890436

24. Nuvolone M, Hermann M, Sorce S, Russo G, Tiberi C, Schwarz P, Minikel E, Sanoudou D, Pelczar P, Aguzzi A. Strictly co-isogenic C57BL/6J-Prnp-/- mice: A rigorous resource for prion science. J Exp Med. 2016 Mar 7;213(3):313–327. PMCID: PMC4813672

25. Gentile J. Divalent siRNA for prion disease. In preparation. 2024.

26. Fischer M, Rülicke T, Raeber A, Sailer A, Moser M, Oesch B, Brandner S, Aguzzi A, Weissmann C. Prion protein (PrP) with amino-proximal deletions restoring susceptibility of PrP knockout mice to scrapie. EMBO J. 1996 Mar 15;15(6):1255–1264. PMCID: PMC450028

27. Jackson WS, Borkowski AW, Faas H, Steele AD, King OD, Watson N, Jasanoff A, Lindquist S. Spontaneous generation of prion infectivity in fatal familial insomnia knockin mice. Neuron. 2009 Aug 27;63(4):438–450. PMCID: PMC2775465

28. Mortberg MA, Gentile JE, Nadaf NM, Vanderburg C, Simmons S, Dubinsky D, Slamin A, Maldonado S, Petersen CL, Jones N, Kordasiewicz HB, Zhao HT, Vallabh SM, Minikel EV. A single-cell map of antisense oligonucleotide activity in the brain. Nucleic Acids Res. 2023 May 16;gkad371. PMID: 37188501

29. Freier SM, Bui HH, Zhao H. Compounds and methods for reducing prion expression [Internet]. WO2020106996A1, 2020 [cited 2021 Jan 22]. Available from: https://patents.google.com/patent/WO2020106996A1/en

30. Vallabh SM, Nobuhara CK, Llorens F, Zerr I, Parchi P, Capellari S, Kuhn E, Klickstein J, Safar JG, Nery FC, Swoboda KJ, Geschwind MD, Zetterberg H, Arnold SE, Minikel EV, Schreiber SL. Prion protein quantification in human cerebrospinal fluid as a tool for prion disease drug development. Proc Natl Acad Sci. 2019 Apr 1;201901947. PMID: 30936307

31. Jafar-Nejad P, Powers B, Soriano A, Zhao H, Norris DA, Matson J, DeBrosse-Serra B, Watson J, Narayanan P, Chun SJ, Mazur C, Kordasiewicz H, Swayze EE, Rigo F. The atlas of RNase H antisense oligonucleotide distribution and activity in the CNS of rodents and non-human primates following central administration. Nucleic Acids Res. 2021 Jan 25;49(2):657–673. PMCID: PMC7826274

32. Petersen RB, Parchi P, Richardson SL, Urig CB, Gambetti P. Effect of the D178N mutation and the codon 129 polymorphism on the metabolism of the prion protein. J Biol Chem. 1996 May 24;271(21):12661–12668. PMID: 8647879

33. Tremblay P, Meiner Z, Galou M, Heinrich C, Petromilli C, Lisse T, Cayetano J, Torchia M, Mobley W, Bujard H, DeArmond SJ, Prusiner SB. Doxycycline control of prion protein transgene expression modulates prion disease in mice. Proc Natl Acad Sci U S A. 1998 Oct 13;95(21):12580–12585. PMCID: PMC22873

34. Mays CE, Kim C, Haldiman T, van der Merwe J, Lau A, Yang J, Grams J, Di Bari MA, Nonno R, Telling GC, Kong Q, Langeveld J, McKenzie D, Westaway D, Safar JG. Prion disease tempo determined by host-dependent substrate reduction. J Clin Invest. 2014 Feb;124(2):847–858. PMCID: PMC3904628

35. Mead S, Gandhi S, Beck J, Caine D, Gajulapalli D, Gallujipali D, Carswell C, Hyare H, Joiner S, Ayling H, Lashley T, Linehan JM, Al-Doujaily H, Sharps B, Revesz T, Sandberg MK, Reilly MM, Koltzenburg M, Forbes A, Rudge P, Brandner S, Warren JD, Wadsworth JDF, Wood NW, Holton JL, Collinge J. A novel prion disease associated with diarrhea and autonomic neuropathy. N Engl J Med. 2013 Nov 14;369(20):1904–1914. PMCID: PMC3863770

36. Mead S, Reilly MM. A new prion disease: relationship with central and peripheral amyloidoses. Nat Rev Neurol. 2015 Feb;11(2):90–97. PMID: 25623792

37. Minikel EV, Vallabh SM, Lek M, Estrada K, Samocha KE, Sathirapongsasuti JF, McLean CY, Tung JY, Yu LPC, Gambetti P, Blevins J, Zhang S, Cohen Y, Chen W, Yamada M, Hamaguchi T, Sanjo N, Mizusawa H, Nakamura Y, Kitamoto T, Collins SJ, Boyd A, Will RG, Knight R, Ponto C, Zerr I, Kraus TFJ, Eigenbrod S, Giese A, Calero M, de Pedro-Cuesta J, Haïk S, Laplanche JL, Bouaziz-Amar E, Brandel JP, Capellari S, Parchi P, Poleggi A, Ladogana A, O'Donnell-Luria AH, Karczewski KJ, Marshall JL, Boehnke M, Laakso M, Mohlke KL, Kähler A, Chambert K, McCarroll S, Sullivan PF, Hultman CM, Purcell SM, Sklar P, van der Lee SJ, Rozemuller A, Jansen C, Hofman A, Kraaij R, van Rooij JGJ, Ikram MA, Uitterlinden AG, van Duijn CM, Exome Aggregation Consortium (ExAC), Daly MJ, MacArthur DG. Quantifying prion disease penetrance using large population control cohorts. Sci Transl Med. 2016 Jan 20;8(322):322ra9. PMCID: PMC4774245

38. Vallabh SM, Zou D, Pitstick R, O'Moore J, Peters J, Silvius D, Kriz J, Jackson WS, Carlson GA, Minikel EV, Cabin DE. Therapeutic Trial of anle138b in Mouse Models of Genetic Prion Disease. J Virol. 2023 Feb 28;97(2):e0167222. PMCID: PMC9973041

39. Jackson WS, Borkowski AW, Watson NE, King OD, Faas H, Jasanoff A, Lindquist S. Profoundly different prion diseases in knock-in mice carrying single PrP codon substitutions associated with human diseases. Proc Natl Acad Sci U S A. 2013 Sept 3;110(36):14759–14764. PMCID: PMC3767526

40. Fischer M, Rülicke T, Raeber A, Sailer A, Moser M, Oesch B, Brandner S, Aguzzi A, Weissmann C. Prion protein (PrP) with amino-proximal deletions restoring susceptibility of PrP knockout mice to scrapie. EMBO J. 1996 Mar 15;15(6):1255–1264. PMCID: PMC450028

41. de Vree PJP, de Wit E, Yilmaz M, van de Heijning M, Klous P, Verstegen MJAM, Wan Y, Teunissen H, Krijger PHL, Geeven G, Eijk PP, Sie D, Ylstra B, Hulsman LOM, van Dooren MF, van Zutven LJCM, van den Ouweland A, Verbeek S, van Dijk KW, Cornelissen M, Das AT, Berkhout B, Sikkema-Raddatz B, van den Berg E, van der Vlies P, Weening D, den Dunnen JT, Matusiak M, Lamkanfi M, Ligtenberg MJL, ter Brugge P, Jonkers J, Foekens JA, Martens JW, van der Luijt R, van Amstel HKP, van Min M, Splinter E, de Laat W. Targeted sequencing by proximity ligation for comprehensive variant detection and local haplotyping. Nat Biotechnol. 2014 Oct;32(10):1019–1025. PMID: 25129690

42. Orrù CD, Groveman BR, Hughson AG, Manca M, Raymond LD, Raymond GJ, Campbell KJ, Anson KJ, Kraus A, Caughey B. RT-QuIC Assays for Prion Disease Detection and Diagnostics. Methods Mol Biol Clifton NJ. 2017;1658:185–203. PMID: 28861791

43. Reidenbach AG, Mesleh MF, Casalena D, Vallabh SM, Dahlin JL, Leed AJ, Chan AI, Usanov DL, Yehl JB, Lemke CT, Campbell AJ, Shah RN, Shrestha OK, Sacher JR, Rangel VL, Moroco JA, Sathappa M, Nonato MC, Nguyen KT, Wright SK, Liu DR, Wagner FF, Kaushik VK, Auld DS, Schreiber SL, Minikel EV. Multimodal small-molecule screening for human prion protein binders. J Biol Chem. 2020 Sept 25;295(39):13516–13531. PMCID: PMC7521658

44. Moore RA, Ward A, Race B, Priola SA. Processing of high-titer prions for mass spectrometry inactivates prion infectivity. Biochim Biophys Acta Proteins Proteomics. 2018;1866(11):1174–1180. PMID: 30282615

45. Hughes CS, Moggridge S, Müller T, Sorensen PH, Morin GB, Krijgsveld J. Single-pot, solid-phase-enhanced sample preparation for proteomics experiments. Nat Protoc. 2019 Jan;14(1):68–85. PMID: 30464214

SUPPLEMENT
PrP turnover in vivo and the time to effect of prion disease therapeutics
Corridon et al 2024

Supplementary Figures

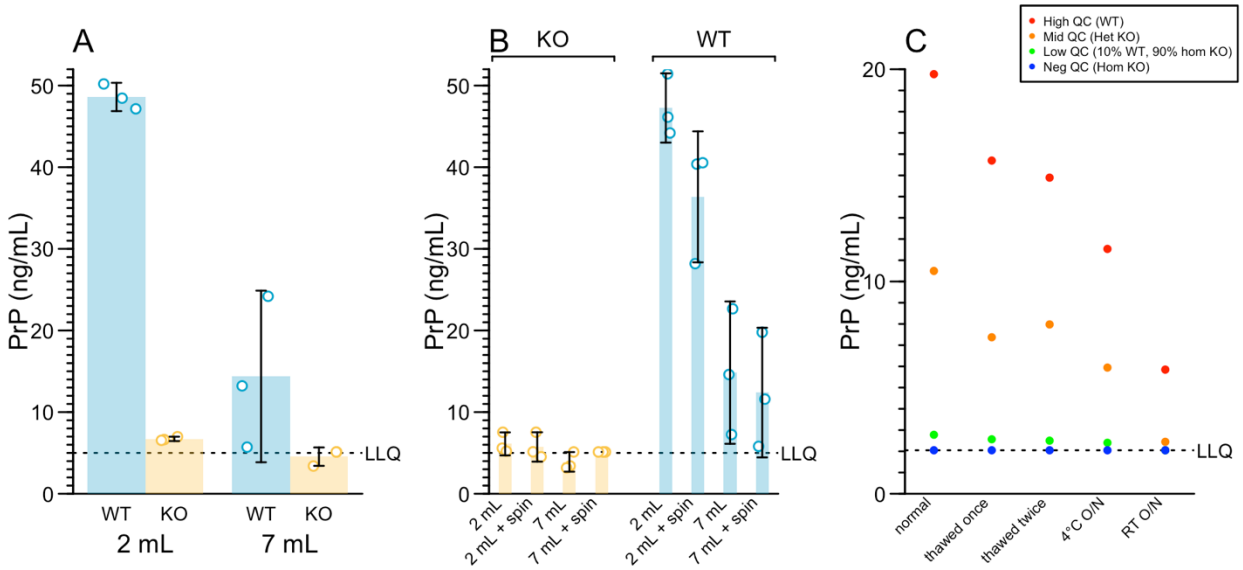

Figure S1. Assay development for ELISA quantification of PrP in colon. A) *Effect of homogenization tubes used. 7 mL tubes homogenize incompletely, leading to lower detection. These data used our standard ELISA conditions with 0.25 µg/mL detection antibody and were conducted at a 1:100 dilution.* ***B)*** *Centrifugation of samples does not rescue the under-recovery of PrP when 7 mL homogenization tubes are used.* ***C)*** *Stability study. PrP in colon samples is subject to loss upon freeze/thaw, time at 4°C or time at room temperature (RT) overnight (O/N). For this stability experiment we treated the lowest standard curve point, 0.02 ng/mL, as the lower limit of quantification (LLQ).*

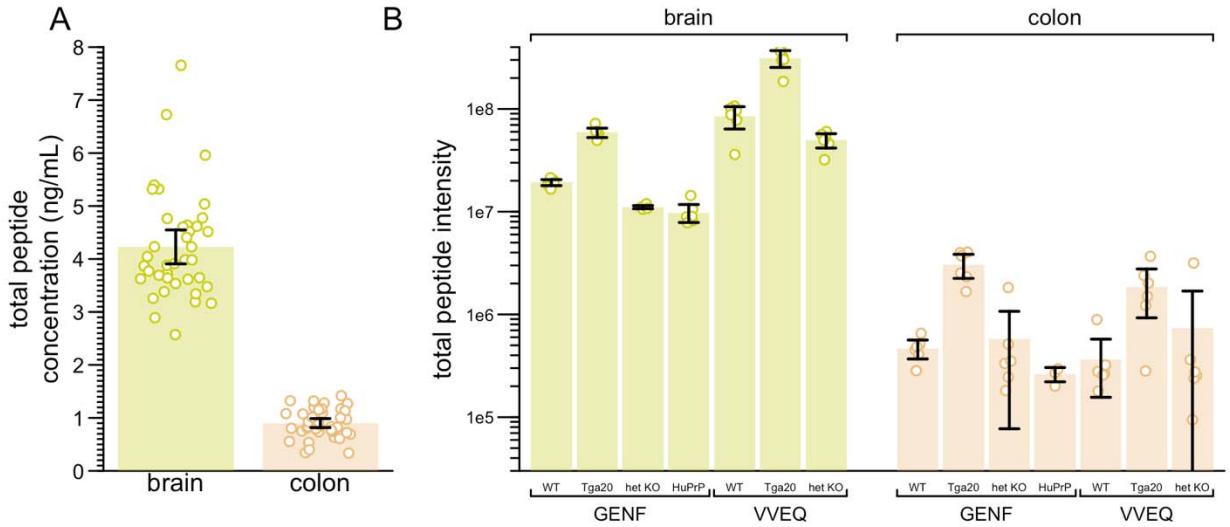

Figure S2. Total abundance of light+heavy peptide in the mass spectrometry assays. A) *The Charles River Labs (CRL) assay for VVEQ. Brain averages 4.7 times higher than colon.* ***B)*** *IQ Proteomics assay for VVEQ and GENF. Brain detection is 19.3 – 231 higher than colon, at odds with our Western and ELISA analysis (Figure 1) and the CRL assay (Figure S1A). Protein in colon may have been under-recovered due to incomplete homogenization. Nonetheless, this does not affect the proportion labeled measurement used in Figure 2.*

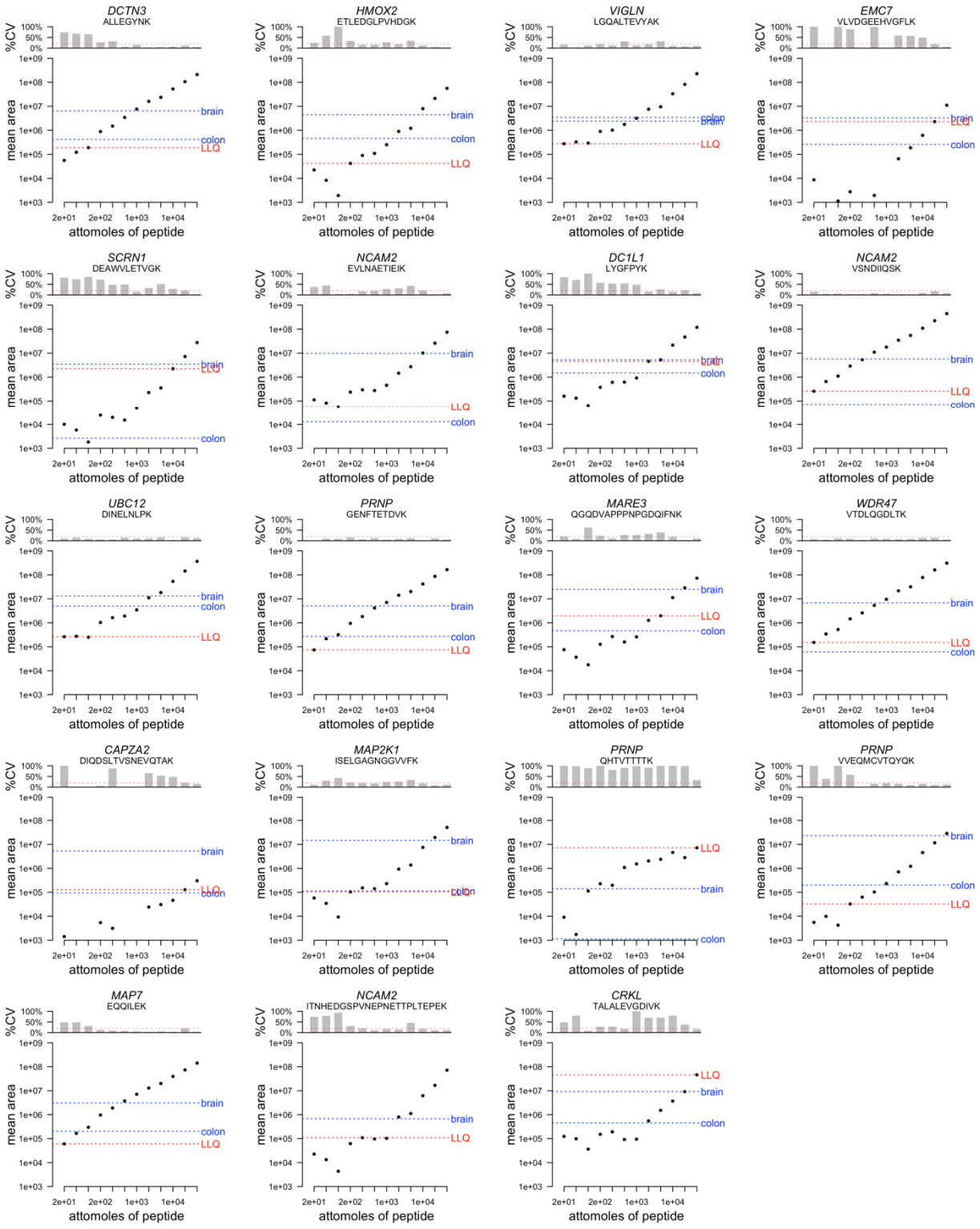

Figure S3. Quality control and LLQ determination for the IQ Proteomics assay. *Each panel represents 1 of 19 peptides, whose identity and gene are shown at top. Synthetic peptides were serially diluted in triplicate. The upper section of each panel shows the coefficient of variation*

(%CV; y axis) among technical replicates at each dilution versus the nominal amount of peptide in amol (attomoles; (x axis shared with lower section). The lower section shows the intensity (y axis) versus nominal amount. We defined each peptide's LLQ (red dashed line) as the most dilute concentration for which the %CV of all concentrations equal or stronger than is ≤20%. Also shown are the mean heavy peptide intensities (blue dashed lines) for wild-type mouse brain and colon at day 8. Thus, if a blue line is above the red line, this means that in wild-type mice after 8 days, the heavy peptide in that tissue is detected above the LLQ.

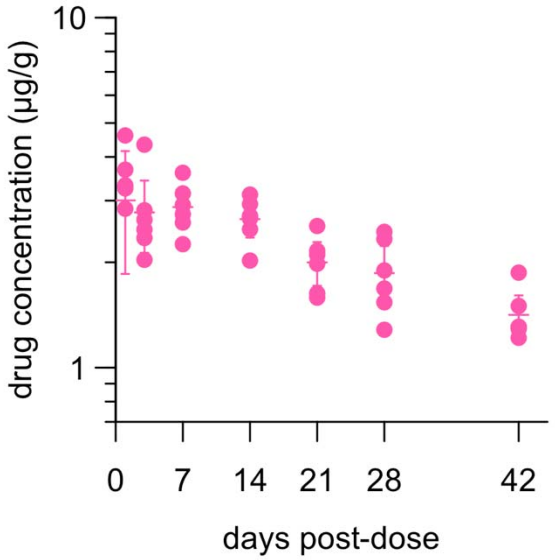

Figure S4. Pharmacokinetic (PK) parameters of ASO N in ki817 mice. *Drug concentration (µg/g, y axis) versus days post-dose (x axis). Points represent individual animals (the same whole hemispheres used for qPCR), line segments represent means, and error bars represent 95% confidence intervals.*

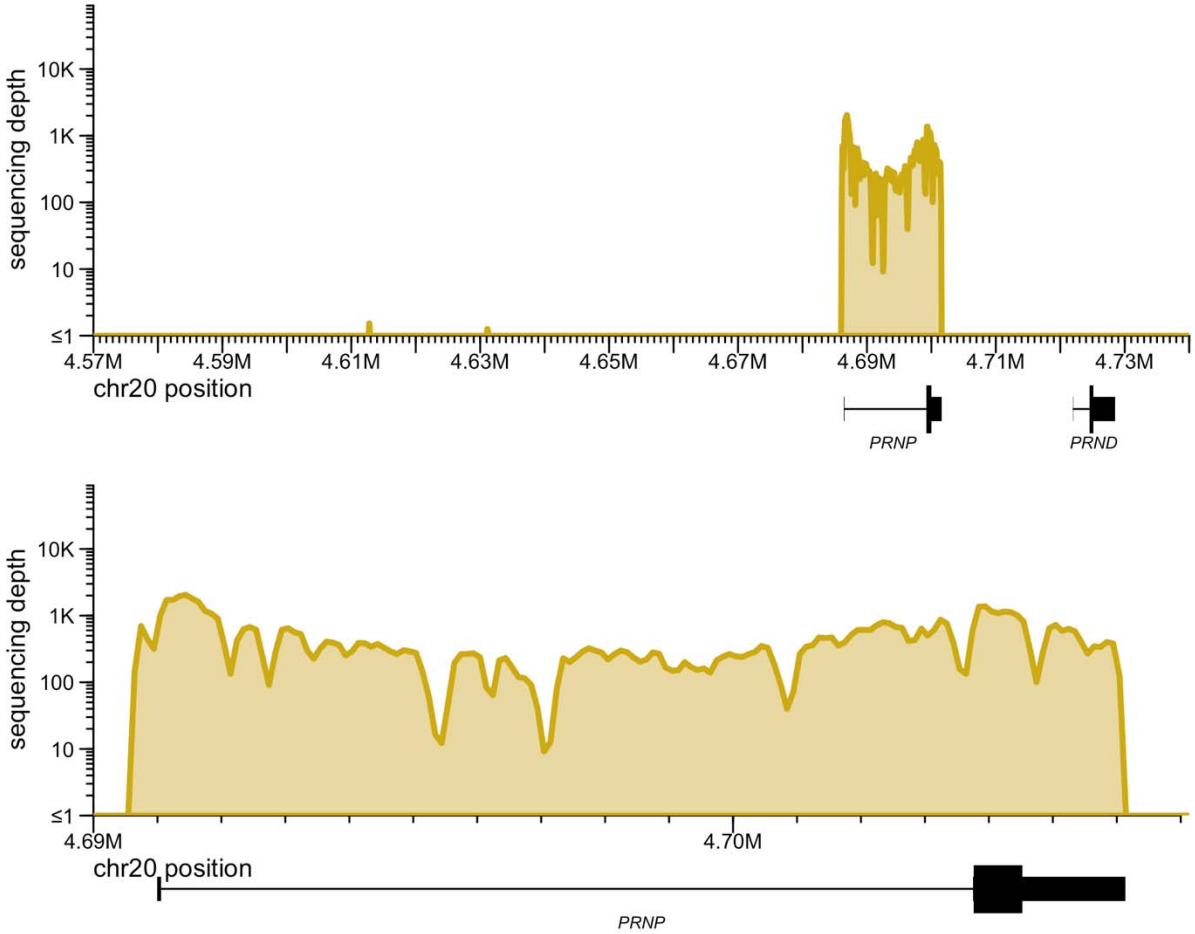

Figure S5. Human genomic sequence in ki817 mice. *Genomic DNA from a ki817 mouse was subjected to targeted sequencing for 152 kb around the PRNP locus using custom baits*[20] *(Twist biosciences) and aligned to the human reference genome. GRCh38 coordinates are shown. The knock-in allele spans 306 bases upstream of the human transcription start site (TSS, located at GRCh38 chr20:4,686,456) to 1 base downstream of the human transcription end site (TES, located at GRCh38 chr20:4701588).*

Sequencing reads demonstrating the breakpoints:

GRCm39 chr2:131751847 (TSS +0 bp) / human GRCh38 chr20:4686151 (TSS -306bp bases upstream of the TSS):
GGCGCGGCCATTGGTGAGCATCACGCCCCGCCCCTCGCCCAGCCTAGCTCCCGCCTGCC
CCGATTAAAGATGATTTTTACAGTCAATGAGCCACGTCAGGGAGCGATGGCACCCGCAGG
CGGTATCAACTGATGCAAGTGTTCAAG

human GRCh38 chr20:4701589 (1 base past the TES) / GRCm39 chr2:131780358 (1 base past TES)
TGAAATTAAACGAGCGAAGATGAGCACCACGGGGTTTGTTCTCTCTCCAATGCTCCGAGTC
CACTGTTTATCGCCAGGGTGGCTTGGGCTCATTTCACATCCCTGTCCCTGAGGGGCCTCG
GGTCTTACCTCTGGTCCTGTCTTGT

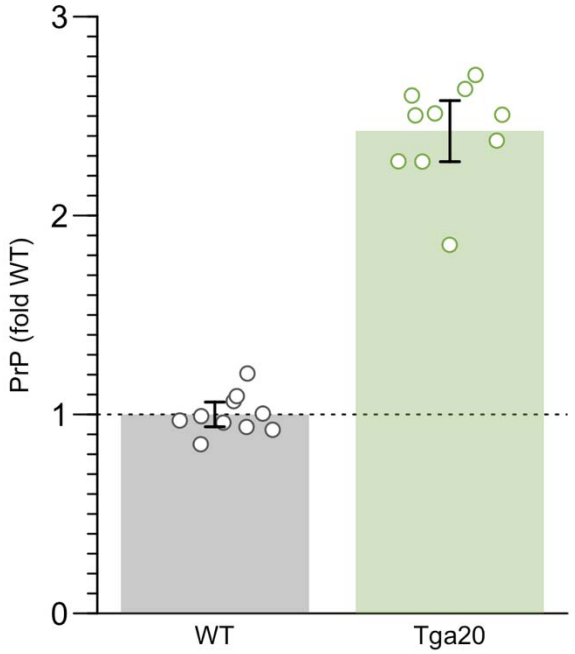

Figure S6. PrP expression in Tga20 mice. *PrP ELISA on whole brain hemisphere homogenates from wild-type C57BL/6N mice or mice hemizygous for the Tga20 transgene array, on a background of endogenous PrP knockout (Tga20/0; ZH3/ZH3). The mean Tga20 value is 2.4x the wild-type result. Transgene mapping of the Tga20 transgene array revealed integration at position (GRCm38) chr17:46,761,775-46,762,856, within intron 1 of Ptcra. The full transgene mapping report is provided in the study's online git repository. The genomic breakpoints were identified as follows:*

5' integration site: GRCm38 chr17:46,761,775 (tail) fused to TG (homologous to chr2:131,909,936 (head))
ATCCCAGCGCCTACACACCCAACACTTCAATCTGTAATGAAATCCTATGCCCTCGTCTAGT
GTGTCTGAAGACACACTCCCGGCTCCCCCGCGTTGTCGGATCAGCAGACCGATTCTGGGC
GCTGCGTCGCATCGGTGGCAGGTAAGCG

3' integration site: TG (homologous to chr2:131,903,786 (head)) fused to GRCm38 chr17:46,762,856 (head) with 3 inserted bases
CTTGTTGGAAGAAGTGTGTAATTGGGGGTGAGCTTTGAAGTTTCAAATGCTTAAGCCAGGC
CCAGTATCACCCTCTCTGCCTTTTTGCTGCCTTTGGATCCGTCGCTTTGGAAATAATCTTTC
TTTTTTTTAAGATTTATTTTATGTAT

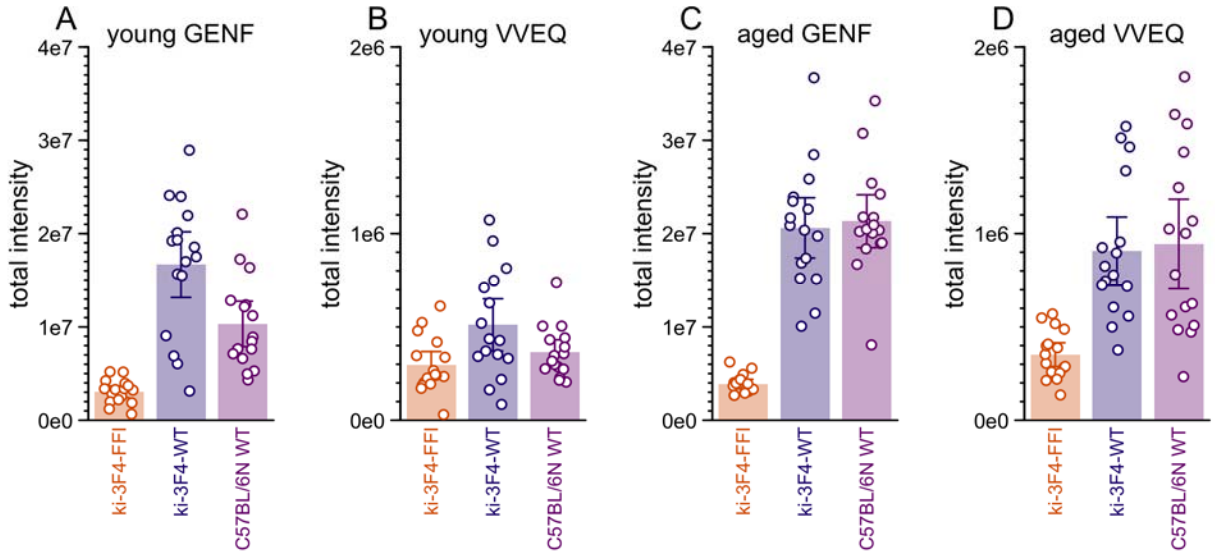

Figure S7. PrP peptide abundance by genotype and age in ki-3F4-FFI mice and controls. *Shown on the y axis are total intensity (heavy + light peptide), grouped by genotype on the x axis; each point is one animal, bars represent means and error bars represent 95% confidence intervals. Age of animals and PrP peptide being monitored are indicated at top of each panel.*

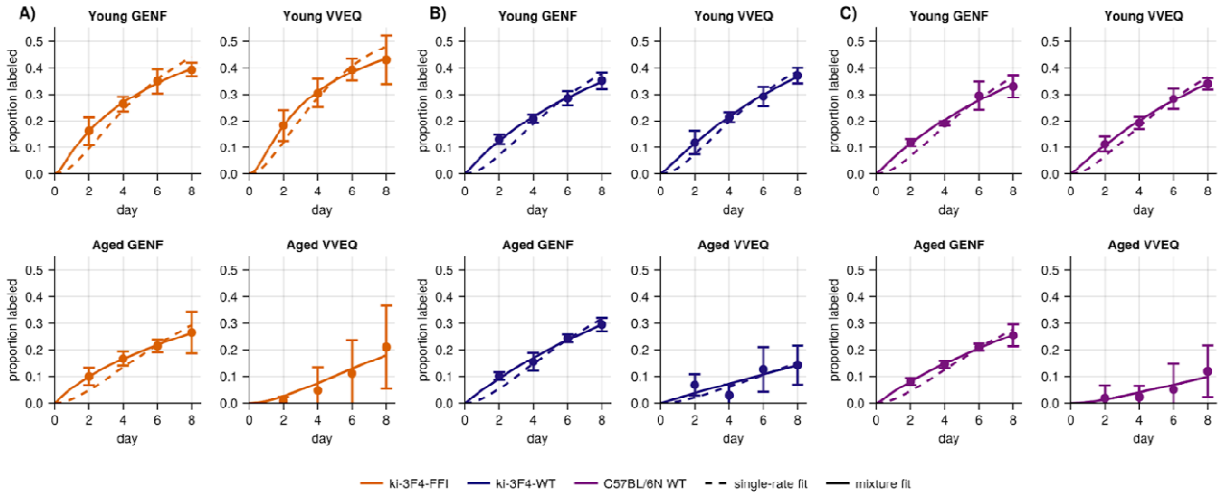

Figure S8. Comparison of single-rate and mixture-of-rates decay models. *For each peptide-age combination the genotypes A) ki-3F4-FFI B) ki-3F4-WT and C) C57BL/6N WT have the label accumulation plotted. Single-rate (dashed line) and mixture-of-rates (solid line) models are shown.*

Supplementary Methods

Targeted mass spectrometry at IQ Proteomics.

Lysis performed at IQ Proteomics. 1mL of lysis buffer containing 8M Urea, 100 mM EPPS pH 8.5, and 1X HALT protease/phosphatase inhibitor (Pierce) was added to each sample. For complete lysis and shearing of genomic DNA, ceramic beads were added to each sample, and the samples were subjected to bead beating (Precellys Evolution) using four cycles at 5800 RPM for 30 seconds, followed by 30 second pause, with active cooling via chilled air circulation to 4°C. SDS was added to 1% w/w, and the lysates were cleared by centrifugation (2 minutes, 1000 x G, 4°C), followed by spin filtration, with an initial pass through 1.2 µM filter (Acroprep Advance, No. 2022-05, PALL Corporation) followed by a second pass through 0.2 µM filter (Acroprep Advance, No. 2022-15, PALL Corporation), after which 6 µL of lysate was removed from each sample into a 96-well plate for the purposes of total protein determination by BCA assay. The remainder of each sample was frozen at -80°C.

Protein Assay. From the reserved 6 µL, each lysate was evaluated via BCA assay (Pierce) according to the manufacturer's protocol. Triplicates at a 1:100 dilution and duplicates at a 1:200 dilution in PBS were incubated with 1X BCA reagent for one hour at 37°C. The samples were assayed for total protein concentration via absorbance at 562 nM in comparison to the standard curve comprised of serially diluted BSA.

Peptide Preparation. 50 µg of total protein (based on BCA assay) was removed from each sample to a new 96-well plate for subsequent processing. Sample volumes were normalized to 50 µL through the addition of the appropriate volume of lysis buffer. DTT was added to 5 mM final concentration in each sample, and samples were incubated at 37°C for 30 minutes. After equilibration to room temperature, iodoacetamide was added to 30 mM final concentration, and the samples were incubated at room temperature (RT) in the dark for 1 hour. Cysteine alkylation was quenched by addition of DTT to a final concentration of 25mM, and the samples were incubated in the dark for an additional 30 minutes at RT.

Digestion. Total protein was isolated via bead-based (SP3) precipitation protocol[45]. Briefly, the magnetic beads were prepared by combining E3 and E7 Sera-Mag Carboxylate-Modified Magnetic SpeedBeads (Cytiva) at 1:1; vol:vol. Beads were washed three times with HPLC water prior to resuspension in lysis buffer for a final bead slurry concentration of 50 µg/µL. 15 µL of the pre-washed bead slurry and 100 µL 100% ethanol were added to each 50 µL sample containing 50 µg of protein. Proteins were allowed to bind and incubate with the bead slurry for 15 min at 25°C with gentle end-over-end rotation. Following protein binding, the supernatant was discarded, and the bead-captured proteins were washed three times with 80% ethanol and air dried. Purified protein-captured beads were resuspended in 100 mM EPPS, pH 8.0. Approximately 50 µg of protein/sample was digested at 25°C for 12 hours with lysyl endopeptidase (LysC, Wako Chemicals USA) at a 1:15; protease:protein (w/w) ratio. Following LysC digestion, the peptides were digested with trypsin at 37°C for 8 hours (Promega) at a 1:25; protease:protein (w/w) ratio. The digested peptides (supernatant) were purified and separated from the magnetic beads. Three post-digestion washes were performed to wash and ensure

elution of all peptides from the beads with the following buffers: 0.2% formic acid, 80% acetonitrile/0.1% formic acid, and 95% acetonitrile/0.1% formic acid. With every wash and elution, the supernatant was transferred and combined with the initial supernatant and dried to completion by vacuum centrifugation. Digested samples were desalted via C18 microextraction (Waters, Product Code 186002318), and peptide eluates were dried via speedvac. Desalted peptides were resuspended in 10uL of 0.2% formic acid for LC-MS analysis.

Preparation of potentially prion-infected for mass spectrometry. For ki-3F4-FFI mice and matched controls, as a precaution in case spontaneously formed prions were present in the brain samples, lysis and sample processing were performed in the prion laboratory at McLaughlin Research Institute and only denatured peptide samples were sent for proteomics, consistent with best practices reported elsewhere[22,44]. Whole brain hemispheres were homogenized at 10% wt/vol in PBS (Gibco 14190) with 2% sodium dodecyl sulfate. A 25 µL aliquot, corresponding to 2.5 mg of tissue or an estimated ~250 µg of input protein, was used for peptide isolation. 25 µL PBS (Gibco 14190) was added, followed by TCEP (Thermo Fisher 77720) to 20 mM final, the solution was incubated at 37°C for 30 minutes, cooled to RT, then iodoacetamide (Sigma A3221) was added to 15 mM final, then incubated at room temperature 60 minutes. TCEP was added again to 40 mM final. Methanol/chloroform precipitation was performed with 100 µL chloroform, 400 µL methanol, and 300 µL water, and centrifugatoion at 3,214 x G for 10 minutes, followed by 2 washes in 200 µL methanol. The protein pellet was air-dried, 10 µL of guanidine hydrochloride was added, transferred to a new microcentrifuge tube, and incubated at 37°C for 30 minutes. 75 µL of 0.2M EPPS pH 8.1 (VWR AAJ612960AE) and 75 µL of HPLC water were added, followed by 5 µg of LysC (Promega V1671), then overnight incubation at room temperature, then 5 µg of trypsin (Promega V5113), and incubation at 37°C for 6 hours. Resulting peptides were frozen at -80°C before advancing to post-digestion wash and desalting steps described above.

LC-MS Data Acquisition. All data were acquired using an Orbitrap Eclipse mass spectrometer equipped with FAIMS-Pro, operating in nano-flow mode using a EASY nanoLC-1200 (ThermoFisher) system (Thermo). Separation was achieved using an in-house packed C18 Column (Sepax GP-C18 resin) that was 30 cm in length with 75 µm inner diameter. Peptides were separated over a gradient composed of Buffer B (80% acetonitrile/0.2% formic acid) in Buffer A (0.2% formic acid) was run according to the following table:

Table S1. LC protocol used at IQ Proteomics.

Time	duration (min)	flow (nL/min)	%B
0	0	300	10
50	50	300	40
55	5	300	100
60	5	300	100

Data was acquired via custom targeted assay with the instrument operating in tMS2 mode. Precursors were isolated using the quadrupole, and fragmented via HCD fragmentation. MS2

spectra were collected in the Orbitrap at 30K resolution. Maximum allowable injection time was set to 300ms.

Table S2. Precursors in the IQ Proteomics assay.

m/z	z	RT Time (min)	Window (min)	HCD Collision Energy (%)	FAIMS CV (V)
874.4391	2	27.5	4	26	-40
877.4491	2	27.5	4	26	-40
614.861	2	41	4	20	-40
617.8711	2	41	4	20	-40
444.2367	2	30	4	20	-55
447.2579	2	30	4	20	-55
454.2478	2	17	4	20	-50
457.2579	2	17	4	20	-50
721.3879	2	30	4	29	-40
724.398	2	30	4	29	-40
705.349	2	20	4	26	-40
708.3591	2	20	4	26	-40
674.367	2	30	4	23	-40
677.377	2	30	4	23	-40
444.2453	2	11	4	17	-45
447.2553	2	11	4	17	-45
961.4738	2	29	4	26	-35
964.4838	2	29	4	26	-35
629.8481	2	30	4	20	-50
632.8582	2	30	4	20	-50
883.4156	3	20	4	29	-55
885.4223	3	20	4	29	-55
502.2746	2	13	4	20	-55
505.2846	2	13	4	20	-55
756.8629	2	19	4	23	-45
759.873	2	19	4	23	-45
570.2644	2	14	4	23	-50
573.2745	2	14	4	23	-50
508.7722	2	5	8	23	-65
511.7823	2	5	8	23	-65
623.8193	2	39	4	26	-50
626.8294	2	30	4	26	-50
528.2902	2	29	4	20	-50

531.3003	2	29	4	20	-50
599.8423	2	25	4	20	-40
596.8322	2	25	4	20	-40
548.303	2	18	4	20	-50
545.293	2	18	4	20	-50
705.2925	2	31	6	23	-45

LC-MS Data Analysis. LC-MS data was analyzed with the Skyline software package (www.skyline.ms). Peptide abundance was calculated as the ratio between the total area under the curve for the endogenous (light), chow-labeled ($^{13}C_6$ heavy) peptides. The following list of transitions was used:

Table S3. Transitions used in the IQ Proteomics assay.

Protein Name	Peptide Sequence	Precursor Mz	Precursor Charge	Product Mz	Product Charge	Fragment Ion	Isotope Label Type
CAPZA2	DIQDSLTVSNEVQTAK	874.439063	2	1189.64229	1	y11	light
CAPZA2	DIQDSLTVSNEVQTAK	874.439063	2	1076.55823	1	y10	light
CAPZA2	DIQDSLTVSNEVQTAK	874.439063	2	975.510551	1	y9	light
CAPZA2	DIQDSLTVSNEVQTAK	874.439063	2	876.442137	1	y8	light
CAPZA2	DIQDSLTVSNEVQTAK	877.449127	2	1195.66242	1	y11	heavy
CAPZA2	DIQDSLTVSNEVQTAK	877.449127	2	1082.57836	1	y10	heavy
CAPZA2	DIQDSLTVSNEVQTAK	877.449127	2	981.53068	1	y9	heavy
CAPZA2	DIQDSLTVSNEVQTAK	877.449127	2	882.462266	1	y8	heavy
CRKL	TALALEVGDIVK	614.861003	2	943.545873	1	y9	light
CRKL	TALALEVGDIVK	614.861003	2	872.50876	1	y8	light
CRKL	TALALEVGDIVK	614.861003	2	759.424696	1	y7	light
CRKL	TALALEVGDIVK	614.861003	2	528.818607	2	y10	light
CRKL	TALALEVGDIVK	614.861003	2	286.176132	1	b3	light
CRKL	TALALEVGDIVK	617.871067	2	949.566002	1	y9	heavy
CRKL	TALALEVGDIVK	617.871067	2	878.528889	1	y8	heavy
CRKL	TALALEVGDIVK	617.871067	2	765.444825	1	y7	heavy
CRKL	TALALEVGDIVK	617.871067	2	531.828671	2	y10	heavy
CRKL	TALALEVGDIVK	617.871067	2	286.176132	1	b3	heavy
DC1L1	LYGFPYK	444.236721	2	774.382102	1	y6	light
DC1L1	LYGFPYK	444.236721	2	407.228896	1	y3	light
DC1L1	LYGFPYK	447.246786	2	780.402231	1	y6	heavy
DC1L1	LYGFPYK	447.246786	2	413.249025	1	y3	heavy
DCTN3	ALLEGYNK	454.247817	2	723.367181	1	y6	light
DCTN3	ALLEGYNK	454.247817	2	610.283117	1	y5	light

DCTN3	ALLEGYNK	454.247817	2	481.240524	1	y4	light
DCTN3	ALLEGYNK	457.257882	2	729.38731	1	y6	heavy
DCTN3	ALLEGYNK	457.257882	2	616.303246	1	y5	heavy
DCTN3	ALLEGYNK	457.257882	2	487.260653	1	y4	heavy
EMC7	VLVDGEEHVGFLK	721.387916	2	1229.61608	1	y11	light
EMC7	VLVDGEEHVGFLK	721.387916	2	1130.54766	1	y10	light
EMC7	VLVDGEEHVGFLK	721.387916	2	1015.52072	1	y9	light
EMC7	VLVDGEEHVGFLK	721.387916	2	615.311677	2	y11	light
EMC7	VLVDGEEHVGFLK	721.387916	2	565.77747	2	y10	light
EMC7	VLVDGEEHVGFLK	724.397981	2	1235.63621	1	y11	heavy
EMC7	VLVDGEEHVGFLK	724.397981	2	1136.56779	1	y10	heavy
EMC7	VLVDGEEHVGFLK	724.397981	2	1021.54085	1	y9	heavy
EMC7	VLVDGEEHVGFLK	724.397981	2	618.321742	2	y11	heavy
EMC7	VLVDGEEHVGFLK	724.397981	2	568.787535	2	y10	heavy
HMOX2	ETLEDGLPVHDGK	705.348988	2	1066.51636	1	y10	light
HMOX2	ETLEDGLPVHDGK	705.348988	2	937.473771	1	y9	light
HMOX2	ETLEDGLPVHDGK	705.348988	2	822.446828	1	y8	light
HMOX2	ETLEDGLPVHDGK	705.348988	2	652.3413	1	y6	light
HMOX2	ETLEDGLPVHDGK	705.348988	2	456.220122	1	y4	light
HMOX2	ETLEDGLPVHDGK	708.359052	2	1072.53649	1	y10	heavy
HMOX2	ETLEDGLPVHDGK	708.359052	2	943.4939	1	y9	heavy
HMOX2	ETLEDGLPVHDGK	708.359052	2	828.466957	1	y8	heavy
HMOX2	ETLEDGLPVHDGK	708.359052	2	658.361429	1	y6	heavy
HMOX2	ETLEDGLPVHDGK	708.359052	2	462.240251	1	y4	heavy
MAP2K1	ISELGAGNGGVVFK	674.366984	2	1018.56801	1	y11	light
MAP2K1	ISELGAGNGGVVFK	674.366984	2	905.483942	1	y10	light
MAP2K1	ISELGAGNGGVVFK	674.366984	2	848.462478	1	y9	light
MAP2K1	ISELGAGNGGVVFK	674.366984	2	777.425364	1	y8	light
MAP2K1	ISELGAGNGGVVFK	677.377048	2	1024.58814	1	y11	heavy
MAP2K1	ISELGAGNGGVVFK	677.377048	2	911.504071	1	y10	heavy
MAP2K1	ISELGAGNGGVVFK	677.377048	2	854.482607	1	y9	heavy
MAP2K1	ISELGAGNGGVVFK	677.377048	2	783.445493	1	y8	heavy
MAP7	EQQILEK	444.245275	2	630.382102	1	y5	light
MAP7	EQQILEK	444.245275	2	502.323525	1	y4	light
MAP7	EQQILEK	444.245275	2	389.239461	1	y3	light
MAP7	EQQILEK	444.245275	2	315.694689	2	y5	light
MAP7	EQQILEK	444.245275	2	386.167024	1	b3	light
MAP7	EQQILEK	447.255339	2	636.402231	1	y5	heavy
MAP7	EQQILEK	447.255339	2	508.343654	1	y4	heavy

MAP7	EQQILEK	447.255339	2	395.25959	1	y3	heavy
MAP7	EQQILEK	447.255339	2	318.704754	2	y5	heavy
MAP7	EQQILEK	447.255339	2	386.167024	1	b3	heavy
MARE3	QGQDVAPPPNPGDQIFNK	961.473771	2	1394.70629	1	y13	light
MARE3	QGQDVAPPPNPGDQIFNK	961.473771	2	1323.66918	1	y12	light
MARE3	QGQDVAPPPNPGDQIFNK	961.473771	2	1226.61641	1	y11	light
MARE3	QGQDVAPPPNPGDQIFNK	961.473771	2	1129.56365	1	y10	light
MARE3	QGQDVAPPPNPGDQIFNK	961.473771	2	918.467957	1	y8	light
MARE3	QGQDVAPPPNPGDQIFNK	964.483836	2	1400.72642	1	y13	heavy
MARE3	QGQDVAPPPNPGDQIFNK	964.483836	2	1329.68931	1	y12	heavy
MARE3	QGQDVAPPPNPGDQIFNK	964.483836	2	1232.63654	1	y11	heavy
MARE3	QGQDVAPPPNPGDQIFNK	964.483836	2	1135.58378	1	y10	heavy
MARE3	QGQDVAPPPNPGDQIFNK	964.483836	2	924.488086	1	y8	heavy
NCAM2	EVLNAETIEIK	629.848092	2	1030.5779	1	y9	light
NCAM2	EVLNAETIEIK	629.848092	2	917.493838	1	y8	light
NCAM2	EVLNAETIEIK	629.848092	2	803.45091	1	y7	light
NCAM2	EVLNAETIEIK	629.848092	2	732.413797	1	y6	light
NCAM2	EVLNAETIEIK	632.858157	2	1036.59803	1	y9	heavy
NCAM2	EVLNAETIEIK	632.858157	2	923.513967	1	y8	heavy
NCAM2	EVLNAETIEIK	632.858157	2	809.471039	1	y7	heavy
NCAM2	EVLNAETIEIK	632.858157	2	738.433926	1	y6	heavy
NCAM2	VSNDIIQSK	502.274563	2	904.473437	1	y8	light
NCAM2	VSNDIIQSK	502.274563	2	817.441408	1	y7	light
NCAM2	VSNDIIQSK	502.274563	2	588.371538	1	y5	light
NCAM2	VSNDIIQSK	502.274563	2	475.287474	1	y4	light
NCAM2	VSNDIIQSK	505.284628	2	910.493566	1	y8	heavy
NCAM2	VSNDIIQSK	505.284628	2	823.461537	1	y7	heavy
NCAM2	VSNDIIQSK	505.284628	2	594.391667	1	y5	heavy
NCAM2	VSNDIIQSK	505.284628	2	481.307603	1	y4	heavy
PRNP	VVEQMC[+57]VTQYQK	756.862894	2	1057.48051	1	y8	light
PRNP	VVEQMC[+57]VTQYQK	756.862894	2	926.440028	1	y7	light
PRNP	VVEQMC[+57]VTQYQK	756.862894	2	667.340966	1	y5	light
PRNP	VVEQMC[+57]VTQYQK	759.872958	2	1063.50064	1	y8	heavy
PRNP	VVEQMC[+57]VTQYQK	759.872958	2	932.460157	1	y7	heavy
PRNP	VVEQMC[+57]VTQYQK	759.872958	2	673.361095	1	y5	heavy
PRNP	GENFTETDVK	570.264393	2	953.457452	1	y8	light
PRNP	GENFTETDVK	570.264393	2	839.414525	1	y7	light
PRNP	GENFTETDVK	570.264393	2	692.346111	1	y6	light
PRNP	GENFTETDVK	570.264393	2	591.298432	1	y5	light

PRNP	GENFTETDVK	573.274457	2	959.477581	1	y8	heavy
PRNP	GENFTETDVK	573.274457	2	845.434654	1	y7	heavy
PRNP	GENFTETDVK	573.274457	2	698.36624	1	y6	heavy
PRNP	GENFTETDVK	573.274457	2	597.318561	1	y5	heavy
PRNP	QHTVTTTTK	508.772188	2	751.41961	1	y7	light
PRNP	QHTVTTTTK	508.772188	2	650.371932	1	y6	light
PRNP	QHTVTTTTK	508.772188	2	450.255839	1	y4	light
PRNP	QHTVTTTTK	508.772188	2	349.208161	1	y3	light
PRNP	QHTVTTTTK	511.782252	2	757.439739	1	y7	heavy
PRNP	QHTVTTTTK	511.782252	2	656.392061	1	y6	heavy
PRNP	QHTVTTTTK	511.782252	2	456.275968	1	y4	heavy
PRNP	QHTVTTTTK	511.782252	2	355.22829	1	y3	heavy
SCRN1	DEAWVLETVGK	623.819335	2	1002.56186	1	y9	light
SCRN1	DEAWVLETVGK	623.819335	2	931.524744	1	y8	light
SCRN1	DEAWVLETVGK	623.819335	2	745.445431	1	y7	light
SCRN1	DEAWVLETVGK	623.819335	2	646.377017	1	y6	light
SCRN1	DEAWVLETVGK	623.819335	2	502.193239	1	b4	light
SCRN1	DEAWVLETVGK	626.8294	2	1008.58199	1	y9	heavy
SCRN1	DEAWVLETVGK	626.8294	2	937.544873	1	y8	heavy
SCRN1	DEAWVLETVGK	626.8294	2	751.46556	1	y7	heavy
SCRN1	DEAWVLETVGK	626.8294	2	652.397146	1	y6	heavy
SCRN1	DEAWVLETVGK	626.8294	2	502.193239	1	b4	heavy
UBC12	DINELNLPK	528.290213	2	827.462144	1	y7	light
UBC12	DINELNLPK	528.290213	2	713.419216	1	y6	light
UBC12	DINELNLPK	528.290213	2	584.376623	1	y5	light
UBC12	DINELNLPK	528.290213	2	471.292559	1	y4	light
UBC12	DINELNLPK	528.290213	2	414.23471	2	y7	light
UBC12	DINELNLPK	531.300278	2	833.482273	1	y7	heavy
UBC12	DINELNLPK	531.300278	2	719.439345	1	y6	heavy
UBC12	DINELNLPK	531.300278	2	590.396752	1	y5	heavy
UBC12	DINELNLPK	531.300278	2	477.312688	1	y4	heavy
UBC12	DINELNLPK	531.300278	2	417.244774	2	y7	heavy
VIGLN	LGQALTEVYAK	596.832245	2	1079.57315	1	y10	light
VIGLN	LGQALTEVYAK	596.832245	2	894.49311	1	y8	light
VIGLN	LGQALTEVYAK	596.832245	2	609.324253	1	y5	light
VIGLN	LGQALTEVYAK	596.832245	2	480.28166	1	y4	light
VIGLN	LGQALTEVYAK	596.832245	2	511.779482	2	y9	light
VIGLN	LGQALTEVYAK	599.84231	2	1085.59328	1	y10	heavy
VIGLN	LGQALTEVYAK	599.84231	2	900.513239	1	y8	heavy

VIGLN	LGQALTEVYAK	599.84231	2	615.344382	1	y5	heavy
VIGLN	LGQALTEVYAK	599.84231	2	486.301789	1	y4	heavy
VIGLN	LGQALTEVYAK	599.84231	2	514.789546	2	y9	heavy
WDR47	VTDLQGDLTK	545.292953	2	990.510216	1	y9	light
WDR47	VTDLQGDLTK	545.292953	2	661.351531	1	y6	light
WDR47	VTDLQGDLTK	545.292953	2	316.150312	1	b3	light
WDR47	VTDLQGDLTK	548.303018	2	996.530345	1	y9	heavy
WDR47	VTDLQGDLTK	548.303018	2	667.37166	1	y6	heavy
WDR47	VTDLQGDLTK	548.303018	2	316.150312	1	b3	heavy

Lower limit of quantification (LLQ) sample preparation. Internal standard peptides labeled with $^{13}C_6$ $^{15}N_2$ lysine (Biosynth, Gardner MA, USA) were mixed into an equimolar solution, and a 12-point, two-fold serial dilution of the peptide mix was prepared by diluting into 0.2% formic acid solution such that the following amounts of peptide were evaluated by LC-MS according to Table S4.

Table S4. Synthetic peptide serial dilutions to determine lower limit of quantification (LLQ)

curve point	fmol peptide on column
12	40
11	20
10	10
9	5
8	2.5
7	1.25
6	0.625
5	0.313
4	0.156
3	0.0781
2	0.039
1	0.0195

LLQ LC-MS Runs. LC and MS instrument parameters for LoQ runs were identical to those for the study samples with the exception that masses corresponding to the heavy synthetic peptide standards (containing terminal $^{13}C_6$ $^{15}N_2$ lysine) were evaluated:

Table S4. Precursors for LLQ determination.

m/z	z	RT Time (min)	Window (min)	HCD Collision Energy (%)	FAIMS CV (V)
874.4391	2	27.7	10	26	-40
878.4462	2	27.7	10	26	-40
614.861	2	40.2	10	20	-40
618.8681	2	40.2	10	20	-40
444.2367	2	31.6	10	20	-55
448.2438	2	31.6	10	20	-55
454.2478	2	20.3	10	20	-50
458.2549	2	20.3	10	20	-50
721.3879	2	30.9	10	29	-40
725.395	2	30.9	10	29	-40
705.349	2	22.1	10	26	-40
709.3561	2	22.1	10	26	-40
674.367	2	30.5	10	23	-40
678.3741	2	30.5	10	23	-40
444.2453	2	13.4	10	17	-45
448.2524	2	13.4	10	17	-45
961.4738	2	29.5	10	26	-35
965.4809	2	29.5	10	26	-35
629.8481	2	31	10	20	-50
633.8552	2	31	10	20	-50
883.4156	3	21.6	10	29	-55
886.087	3	21.6	10	29	-55
502.2746	2	15.2	10	20	-55
506.2817	2	15.2	10	20	-55
400.2554	2	30.7	10	20	-60
405.2596	2	30.7	10	20	-60
522.7409	2	10	10	20	-55
527.745	2	10	10	20	-55
778.3658	2	27.4	10	23	-40
783.3699	2	27.4	10	23	-40
544.7358	2	10.8	10	20	-60
549.7399	2	10.8	10	20	-60
756.8629	2	21.1	10	23	-45
760.87	2	21.1	10	23	-45

570.2644	2	16	10	23	-50
574.2715	2	16	10	23	-50
508.7722	2	7.5	10	23	-65
512.7793	2	7.5	10	23	-65
545.2572	2	8.8	10	32	-60
550.2614	2	8.8	10	32	-60
623.8193	2	37.9	10	26	-50
627.8264	2	37.9	10	26	-50
483.238	2	18	10	26	-50
488.2421	2	18	10	26	-50
525.8084	2	43.5	10	20	-55
530.8125	2	43.5	10	20	-55
528.2902	2	29.7	10	20	-50
532.2973	2	29.7	10	20	-50
596.8322	2	26.7	10	20	-40
600.8393	2	26.7	10	20	-40
545.293	2	19.7	10	20	-50
549.3001	2	19.7	10	20	-50

Table S6. Fragment ions corresponding to the synthetic peptides for LLQ determination.

Peptide	Precursor m/z	Fragment m/z	Fragment Ion
DIQDSLTVSNEVQTAK	878.446162	1197.65649	y11
DIQDSLTVSNEVQTAK	878.446162	1084.57243	y10
DIQDSLTVSNEVQTAK	878.446162	983.52475	y9
DIQDSLTVSNEVQTAK	878.446162	884.456336	y8
TALALEVGDIVK	618.868102	951.560072	y9
TALALEVGDIVK	618.868102	880.522959	y8
TALALEVGDIVK	618.868102	767.438895	y7
TALALEVGDIVK	618.868102	532.825706	y10
LYGFPYK	448.243821	782.396301	y6

LYGFPYK	448.243821	619.332973	y5
LYGFPYK	448.243821	562.311509	y4
LYGFPYK	448.243821	415.243095	y3
LYGFPYK	448.243821	391.701789	y6
ALLEGYNK	458.254917	731.38138	y6
ALLEGYNK	458.254917	618.297316	y5
ALLEGYNK	458.254917	489.254723	y4
VLVDGEEHVGFLK	725.395016	1237.63028	y11
VLVDGEEHVGFLK	725.395016	1138.56186	y10
VLVDGEEHVGFLK	725.395016	1023.53492	y9
VLVDGEEHVGFLK	725.395016	619.318777	y11
VLVDGEEHVGFLK	725.395016	569.78457	y10
ETLEDGLPVHDGK	709.356087	1074.53056	y10
ETLEDGLPVHDGK	709.356087	945.48797	y9
ETLEDGLPVHDGK	709.356087	830.461027	y8
ETLEDGLPVHDGK	709.356087	660.355499	y6
ETLEDGLPVHDGK	709.356087	464.234321	y4
ISELGAGNGGVVFK	678.374083	1026.58221	y11
ISELGAGNGGVVFK	678.374083	913.498141	y10
ISELGAGNGGVVFK	678.374083	856.476677	y9
ISELGAGNGGVVFK	678.374083	785.439563	y8
EQQILEK	448.25237	638.39630	y5

	4	1	
EQQILEK	448.252374	510.337724	y4
EQQILEK	448.252374	397.25366	y3
EQQILEK	448.252374	319.701789	y5
EQQILEK	448.252374	386.167024	b3
QGQDVAPPPNPGDQIFNK	965.480871	1402.72049	y13
QGQDVAPPPNPGDQIFNK	965.480871	1331.68338	y12
QGQDVAPPPNPGDQIFNK	965.480871	1234.63061	y11
QGQDVAPPPNPGDQIFNK	965.480871	1137.57785	y10
QGQDVAPPPNPGDQIFNK	965.480871	926.482156	y8
EVLNAETIEIK	633.855192	1038.5921	y9
EVLNAETIEIK	633.855192	925.508037	y8
EVLNAETIEIK	633.855192	811.465109	y7
EVLNAETIEIK	633.855192	740.427996	y6
EVLNAETIEIK	633.855192	611.385402	y5
ITNHEDGSPVNEPNETTPLTEPEK	886.086987	1363.6831	y12
ITNHEDGSPVNEPNETTPLTEPEK	886.086987	821.449459	y7
ITNHEDGSPVNEPNETTPLTEPEK	886.086987	1293.57059	b12
VSNDIIQSK	506.281663	912.487636	y8
VSNDIIQSK	506.281663	825.455607	y7
VSNDIIQSK	506.281663	711.41268	y6
VSNDIIQSK	506.281663	596.385737	y5

VSNDIIQSK	506.281663	483.301673	y4
VVEQMC[+57.021464]VTQYQK	760.869993	1065.49471	y8
VVEQMC[+57.021464]VTQYQK	760.869993	934.454227	y7
VVEQMC[+57.021464]VTQYQK	760.869993	675.355165	y5
GENFTETDVK	574.271492	961.471651	y8
GENFTETDVK	574.271492	847.428724	y7
GENFTETDVK	574.271492	700.36031	y6
GENFTETDVK	574.271492	599.312631	y5
QHTVTTTTK	512.779287	759.433809	y7
QHTVTTTTK	512.779287	658.386131	y6
QHTVTTTTK	512.779287	559.317717	y5
QHTVTTTTK	512.779287	458.270038	y4
QHTVTTTTK	512.779287	357.22236	y3
DEAWVLETVGK	627.826435	1010.57606	y9
DEAWVLETVGK	627.826435	939.538943	y8
DEAWVLETVGK	627.826435	753.45963	y7
DEAWVLETVGK	627.826435	654.391216	y6
DEAWVLETVGK	627.826435	502.193239	b4
DINELNLPK	532.297313	835.476343	y7
DINELNLPK	532.297313	721.433415	y6
DINELNLPK	532.297313	592.390822	y5
DINELNLPK	532.29731	479.30675	y4

	3	8	
DINELNLPK	532.297313	418.241809	y7
LGQALTEVYAK	600.839345	1087.58735	y10
LGQALTEVYAK	600.839345	902.507309	y8
LGQALTEVYAK	600.839345	831.470195	y7
LGQALTEVYAK	600.839345	718.386131	y6
LGQALTEVYAK	600.839345	515.786581	y9
VTDLQGDLTK	549.300053	998.524415	y9
VTDLQGDLTK	549.300053	897.476737	y8
VTDLQGDLTK	549.300053	669.36573	y6
VTDLQGDLTK	549.300053	541.307152	y5
VTDLQGDLTK	549.300053	316.150312	b3

Targeted mass spectrometry at Charles River Labs.

Tissue homogenization. Colon and brain tissue were homogenized in TPER reagent (Thermo No. 78510) with 1X HALT protease inhibitor (Thermo No. 78430) at a ratio of 1 g tissue to 9 mL buffer.

Total protein estimation by BCA assay. 10 µL aliquots of tissue homogenates (see above) were diluted 10-fold in water for total protein estimation. Seven calibration standards concentrations (2, 1, 0.5, 0.25, 0.125, 0.0625, 0.03125) were prepared with serial 2x dilution in milliQ water. BCA reagent was prepared by mixing reagent A and B in a 50:1 ratio. 20 µL of sample and 200 µL of BCA reagent were added to each well of a clear bottom 96 well plate and incubated at 37°C for 20 minutes. Absorbance of each well was read at 562 nm using a UV spectrometer. Samples were diluted to 3 mg/mL total protein concentration based on BCA assay data.

Extraction procedure. 60 µL of mixed reagent consisting of 20 µL bovine serum albumin (BSA), 30 µL ammonium bicarbonate (ABC, 100 mM), and 10 µL dithiothreitol (DTT, 250 mM) was added to 80 µL of the 3 mg/mL sample and mixed before incubating at 95°C for 10 minutes at 300 rpm shaking. Samples were then allowed to cool for 10 minutes at room temperature. 10 µL of iodoacetamide (IAA, 500 mM) was added to the samples, vortexed to mix and incubated at RT in the dark for 30 minutes. 1 mL of cold acetone was added to the samples and vortexed to mix again prior to incubating at -80°C for 30 minutes. Samples were spun at 16,000 x G for 5 minutes and supernatant was discarded. The protein pellet was dried in the hood, washed with 500 µL cold methanol and dried for 30 additional minutes in the hood at room temperature. The protein pellet was resuspended in 60 µL of 50 mM ABC plus 20 µL of diluted trypsin (0.16 µg/µL) for a final quantity of 3.2 µg trypsin to 240 µg protein (1:75 enzyme:protein ratio) and mixed with a pipette before incubating for 16 hours at 37°C. An internal standard (IS) of peptide with isotopically labeled lysine (^{13}C, ^{15}N) custom synthesized by Vivitide was used. The reaction was stopped by adding 10 µL of IS (prepared in 0.5% FA ACN-H_2O 80:20) and 10 µL FA in ACN:H_2O (80:20) and vortexing to mix before centrifugation at 8,000 x G for 5 minutes. Supernatants were transferred to LCMS vials.

Calibration curve. 80 µL of 50 mM ammonium bicarbonate was aliquoted into the tubes designated for blanks and standards. The calibration curve was prepared with light peptides standard custom synthesized by Vivitide. 10 µL of ACN:H2O:FA 1:10:1 was aliquoted into each 80 µL sample, blank, or standard. 10 µL of standards were added to tubes labeled for standards. 10 µL of IS in 80:20:0.5 ACN:H_2O:FA was added to all standard, QC, and blank tubes except for double blank tubes. 10 µL of 80:20:0.5 ACN:H_2O:FA was added to double blanks. All Eppendorf tubes were covered and vortexed prior to being centrifuged for 5 minutes at 8000 x G. At least 80 µL of the samples were transferred into a clean 96-well plate.